

## SIMULTANEOUS OPTICAL AND NEAR-INFRARED SPECTROPOLARIMETRY OF TYPE 2 SEYFERT GALAXIES

MAKOTO WATANABE,<sup>1</sup> TETSUYA NAGATA, AND SHUJI SATO  
Department of Physics, Nagoya University, Furo-cho, Chikusa-ku, Nagoya 464-8602, Japan

HIDEHIKO NAKAYA  
Subaru Telescope, National Astronomical Observatory of Japan, 650 North A'ohoku Place, Hilo, HI 96720

AND

J. H. HOUGH  
Division of Physical Sciences, University of Hertfordshire, College Lane, Hatfield, Hertfordshire AL10 9AB, UK  
*Received 2002 December 12; accepted 2003 March 24*

### ABSTRACT

We present optical and near-infrared spectropolarimetry of the nuclei of four type 2 Seyfert galaxies, Mrk 463E, Mrk 1210, NGC 1068, and NGC 4388. The data were obtained simultaneously, covering the wavelength range of 0.46–2.5  $\mu\text{m}$ . We model the polarizations from two dust-scattering components: (1) scattering in dusty regions in ionization cones and (2) scattering in a torus surrounding a type 1 nucleus. The polarizations from electron scattering in the cones and dichroic absorption by aligned dust grains in the torus are also compared with the observations. We confirmed that a combination of electron and dust scattering in the ionization cones is the preferred mechanism for the optical continuum polarization. For the near-infrared, dichroic absorption by aligned grains can explain the continuum polarization of Mrk 463E and Mrk 1210 as well as NGC 1068. Visual optical depths of the order of 10–20 are estimated for dichroic absorption in these nuclei. Dust scattering in the torus, whose grain size distribution is assumed to be the same as in the Galactic diffuse interstellar medium, cannot reproduce the observed spectral slope of the near-infrared polarization and total nuclear flux simultaneously. However, this might only indicate that the grain size distribution in the torus of active galactic nuclei (AGNs) is different, and dust scattering with moderate optical depth and dominated by large grains might provide a reasonable explanation for the near-infrared radiation from AGNs.

*Subject headings:* galaxies: nuclei — galaxies: Seyfert — infrared: galaxies — polarization

### 1. INTRODUCTION

According to the current unified model for Seyfert galaxies (see Antonucci 1993 for a review), all types of Seyfert galaxies have a type 1 nucleus (featureless continuum sources and broad-line regions [BLRs]), surrounded by an optically and geometrically thick dusty and molecular torus. In addition, cone-shaped ionization regions exist along the polar axis of the torus as narrow-line regions (NLRs; see Wilson 1996 for a review). The difference between type 1 (broad permitted lines) and type 2 (narrow permitted lines) occurs because of the obscuration of our view of the nucleus by the torus. In type 2 Seyfert galaxies, however, the radiation from the obscured nucleus can be observed in the polarized flux spectrum by scattering in the cones.

Antonucci & Miller (1985) proposed electron scattering as the principal polarization mechanism on the basis of the flatness of the degree of continuum polarization. Miller & Antonucci (1983) and Antonucci & Miller (1985) showed that the degree of the continuum polarization of the type 2 Seyfert NGC 1068 is constant ( $\sim 16\%$ ) over the UV and optical wavelengths, after correction for starlight dilution. Subsequently, many authors confirmed that electron scattering dominates the UV and optical polarization of the nuclei of many type 2 Seyfert galaxies (Miller & Goodrich 1990; Tran, Miller, & Kay 1992; Tran 1995a, 1995b). On the

other hand, the degree of polarization of NGC 1068 rises toward 2  $\mu\text{m}$  in the near-infrared (Bailey et al. 1988; Young et al. 1995). Young et al. (1995) proposed that dichroic absorption by aligned dust grains in the torus dominates the near-infrared polarization of NGC 1068. This mechanism has been also modeled for some other type 2 active galactic nuclei (AGNs; Young et al. 1996a, 1996b).

However, dust scattering is also likely to contribute additionally to the polarization of some type 2 Seyfert nuclei. Miller, Goodrich, & Mathews (1991) found a highly polarized region that shows a rapid rise in the degree of polarization toward the blue at about 5'' from the nucleus of NGC 1068. Miller & Goodrich (1990) and Tran (1995b) found that the degree of the continuum polarization of Mrk 463E also rises toward the blue, even after correction for starlight dilution, and suggested dust scattering as the most likely cause. Tran (1995b) identified a possible knot near the nucleus of Mrk 463E responsible for the dust scattering.

Furthermore, the dusty torus itself may produce some degree of polarization in the near-infrared. The recent most successful torus models that can well reproduce the infrared spectra of AGNs require moderate visual torus extinctions ( $A_V = 10\text{--}80$ ) along our lines of sight to the central regions for type 2 Seyfert nuclei (Granato, Danese, & Franceschini 1997; Fadda et al. 1998). These moderate extinctions enable us to observe the central regions directly through the tori in the near-infrared because of the decrease of extinction at these wavelengths. The detection of the near-infrared broad emission lines in some type 2 Seyfert nuclei (Rix et al. 1990; Blanco, Ward, & Wright 1990; Goodrich, Veilleux, & Hill

<sup>1</sup>Current address: Subaru Telescope, National Astronomical Observatory of Japan, 650 North A'ohoku Place, Hilo, HI 96720; watanabe@naoj.org.

1994; Ruiz, Rieke, & Schmidt 1994; Veilleux, Goodrich, & Hill 1997) also supports a direct view of the central regions (BLRs) of the nuclei at these wavelengths. Tori with moderate extinction may also produce polarization through scattered light. However, the polarization from dust scattering in the torus, including the wavelength dependence, is not well studied, and only a few authors have modeled this (Kartje 1995; Wolf & Henning 1999).

The relative importance of these various polarization mechanisms is best investigated by polarimetry over a very wide spectral range. Therefore, we here made simultaneous optical and near-infrared polarimetry and investigated, in particular, the influence of dust scattering on the polarization of type 2 Seyfert nuclei. In this paper we present spectropolarimetry of the nuclei of four type 2 Seyfert galaxies, Mrk 463E, Mrk 1210, NGC 1068, and NGC 4388, which are known to have obscured type 1 nuclei. We also present the model polarization spectra produced by dust scattering in dusty regions within the ionization cones and in a torus and compare these with the observations. Section 2 describes the observations and data reduction, and § 3 presents the observational results. In § 4 we present the polarization models and spectra and compare them with the observations. In § 5 we discuss dust scattering in type 2 Seyfert nuclei. Section 6 presents our conclusions.

## 2. OBSERVATIONS AND DATA REDUCTION

### 2.1. Observations

All observations were obtained at the 3.8 m United Kingdom Infrared Telescope (UKIRT), Mauna Kea, Hawaii, on 2000 August 25 and 2001 February 21 and March 23 UT. The Triple Range Imager and Spectrograph (TRISPEC; Sato 2000), developed at Nagoya University, and IRPOL2 were used. TRISPEC has two dichroic mirrors splitting a spectrum to one optical channel (0.46–0.90  $\mu\text{m}$ ) and two infrared channels (0.92–1.80 and 1.88–2.50  $\mu\text{m}$ ). For the optical channel, a SITe  $512 \times 512$  pixel CCD with a pixel scale of  $0''.11 \text{ pixel}^{-1}$  was used. For the infrared channels, two SBRC  $256 \times 256$  pixel InSb arrays with a pixel scale of  $0''.22 \text{ pixel}^{-1}$  were used. The three spectra were obtained simultaneously, covering the wavelength range of 0.46–2.5  $\mu\text{m}$ .

Three gratings with 200, 120, and 150 lines  $\text{mm}^{-1}$  were used, giving dispersions of 12, 46, and 31  $\text{\AA} \text{ pixel}^{-1}$  for the optical and two infrared channels, respectively. For all observations, an aperture mask containing two slits with a width of  $0''.88$  and a length of  $12''$  was used. The spectral

resolution ( $\lambda/\Delta\lambda$ ) was 69, 71, and 180 at 0.665, 1.30, and 2.22  $\mu\text{m}$ , respectively. The slits were oriented north-south on the sky. The location, size, and orientation of the aperture were exactly identical for all three channels, because the aperture mask was placed in front of both dichroic mirrors.

For spectropolarimetry, three cold Wollaston prisms and a warm superachromatic half-wave retarder (0.36–2.5  $\mu\text{m}$ ), provided by University of Hertfordshire, were used. The Wollaston prisms form ordinary and extraordinary images of the two slits. For each object, eight exposures were taken as two sets of four frames with retarder positions of  $0^\circ$ ,  $45^\circ$ ,  $22.5^\circ$ , and  $67.5^\circ$ . Each set consists of four pairs of orthogonally polarized spectra. The regions of the sky near the objects were also obtained with the four retarder positions, with the distance from the object  $28''$ ,  $60''$ ,  $300''$ , and  $60''$  along the north-south direction for Mrk 463E, Mrk 1210, NGC 1068, and NGC 4388, respectively.

Table 1 shows the journal of observations with the seeing, estimated at 0.55  $\mu\text{m}$  (FWHM) from observations of standard stars.

### 2.2. Data Reduction and Corrections

The data were reduced using IRAF<sup>2</sup> and our reduction package TRISPEC. Uncertainties due to Poisson statistics and detector readout noises were propagated at every step of the reduction process, yielding error spectra for Stokes parameters. Dome flats were taken using a tungsten-halogen lamp, to provide the flat fields. The window size of spectral extraction was  $2''.5$ – $3''.5$  (Table 1) along the slit, depending on the seeing. The wavelengths were calibrated using a mercury-argon lamp. The flux calibrations and removal of atmospheric absorption features were achieved by the observation of BS 311, BS 3650, and BS 5384, using the stellar spectra from Pickles (1998) as templates. The zero points of the position angle (P.A.) of polarization were determined from the observations of the polarized stars CMa R1 No. 24, HD 38563C, and Cyg OB2 No. 5 in Whittet et al. (1992). The polarization efficiency of the system was checked by observing BS 8845 through a Glan prism on 2000 August 24 UT, giving 99.5%, 97%, and 99% at 0.665, 1.30, and 2.22  $\mu\text{m}$ , respectively. The bias in the

<sup>2</sup> IRAF is distributed by the National Optical Astronomy Observatory, which is operated by the Association of Universities for Research in Astronomy, Inc., under cooperative agreement with the National Science Foundation.

TABLE 1  
JOURNAL OF SPECTROPOLARIMETRIC OBSERVATIONS

OBJECT	UT DATE	EXPOSURE (s)		SEEING <sup>a</sup> (arcsec)	EXTRACTION <sup>b</sup> (arcsec)
		Optical	NIR		
Mrk 463E.....	2001 Feb 21	1936	1920	1.3–1.4	3.0
Mrk 1210.....	2001 Mar 23	1936	1920	0.9–1.1	2.5
NGC 1068.....	2000 Aug 25	1768	1440	1.3–1.5	3.5
NGC 4388.....	2001 Mar 23	1936	1920	0.8–0.9	2.5

<sup>a</sup> FWHM estimated from observations of standard stars.

<sup>b</sup> Window size of the spectral extraction.

TABLE 2  
GALACTIC INTERSTELLAR REDDENING AND POLARIZATION

OBJECT	REDSHIFT <sup>a</sup>	$E(B-V)$ <sup>b</sup>	PROBE <sup>c</sup>	SEPARATION <sup>d</sup> (arcmin)	ADOPTED SERKOWSKI CURVE PARAMETERS			
					$K$	$P_{\max}$ (%)	$\theta$ (deg)	$\lambda_{\max}$ ( $\mu\text{m}$ )
Mrk 463E.....	0.05000	0.030	PPM 130144 <sup>e</sup>	68	0.69	0.244	67	0.4905
Mrk 1210.....	0.01350	0.030	HD 66665	65	1.15	0.110	34.6	0.545
NGC 1068.....	0.00379	0.034	HD 16582	52	1.15	0.071	162.0	0.545
NGC 4388.....	0.00842	0.033	HD 106929	192	1.15	0.210	55.7	0.545

<sup>a</sup> From the NASA/IPAC Extragalactic Database (NED).

<sup>b</sup> From Schlegel et al. 1998.

<sup>c</sup> Probe stars from Heiles 2000 to estimate the interstellar polarization. Only  $P_{\max}$  and  $\theta$  are taken.

<sup>d</sup> Spatial separation between the object and probe star in the plane of the sky.

<sup>e</sup> All parameters are from Tran 1995a.

degree of polarization due to the noise was reduced by

$$P = \begin{cases} (P_{\text{obs}}^2 - \sigma_P^2)^{1/2} & P_{\text{obs}}^2 - \sigma_P^2 \geq 0, \\ 0 & P_{\text{obs}}^2 - \sigma_P^2 < 0, \end{cases}$$

where  $P_{\text{obs}}$  is the observed degree of polarization and  $\sigma_P$  is the uncertainty in  $P_{\text{obs}}$ .

After the basic data reduction described above, the effects of reddening and polarization due to the Galactic interstellar medium were calculated. The amounts of interstellar reddening were estimated from the dust map of Schlegel, Finkbeiner, & Davis (1998). The values of  $E(B-V)$  derived from their map for our objects are presented in Table 2. By assuming  $R_V = 3.1$  and the interstellar reddening curve of Cardelli, Clayton, & Mathis (1989), the flux spectra of our objects were corrected. For all of our objects, this correction is rather small because of the small values of  $E(B-V)$ . The degrees of interstellar polarization were estimated from previous polarimetry of stars close to the line of sight to our objects. Except for Mrk 463E, the stars were selected from the polarization catalogs in Heiles (2000). For Mrk 463E, the stellar polarization measured by Tran (1995a) was adopted. Table 2 shows the selected stars and the polarization. For the wavelength dependence of interstellar polarization, we assumed the Serkowski curve (Serkowski, Mathewson, & Ford 1975; Wilking et al. 1980):

$$P_\lambda = P_{\max} \exp[-K \ln^2(\lambda_{\max}/\lambda)],$$

where  $P_\lambda$  is the degree of polarization at the wavelength  $\lambda$ ,  $P_{\max}$  is the maximum polarization that occurs at  $\lambda_{\max}$ , and  $K$  is the parameter for the width of the curve. Adopting the parameters in Table 2, the interstellar polarization was subtracted from the observed polarization in the  $Q$  and  $U$  Stokes parameter space. Except for PPM 130144, from Tran (1995a), we assumed  $K = 1.15$  and  $\lambda_{\max} = 0.545 \mu\text{m}$ , because measured values of these parameters were unavailable. These values of  $K$  and  $\lambda_{\max}$  are typical of those found by Serkowski et al. (1975) for the standard interstellar medium. This value of  $\lambda_{\max}$  corresponds to  $R_V = 3.1$  (Whittet & van Breda 1978). We also assumed that the optical polarizations in Heiles (2000) are near  $P_{\max}$ .

### 3. OBSERVATIONAL RESULTS

Figures 1–4 show the spectropolarimetric results for NGC 1068, Mrk 468E, Mrk 1210, and NGC 4388 after

correction for the Galactic reddening and interstellar polarization. All spectra are shown in the rest frame of the object. For NGC 4388, only the optical spectra are shown, because there was insufficient signal-to-noise ratio (S/N) to obtain good spectra in the near-infrared. For Mrk 1210 and NGC 4388, the polarization spectra are binned to reduce the noise.

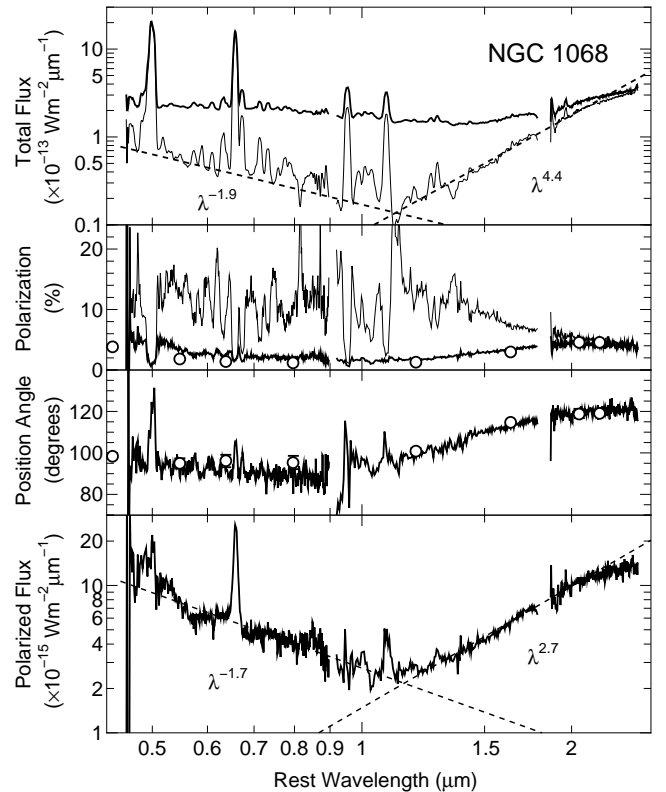


FIG. 1.—Spectropolarimetry of NGC 1068. From top to bottom are the total flux  $F_\lambda$ , the degree of polarization  $P$ , the position angle of polarization  $\theta$ , and the polarized flux  $P \times F_\lambda$  as a function of wavelength after correction for the Galactic interstellar reddening and polarization (thick solid curves). The thin solid curves in the top two panels show  $F_\lambda$  and  $P$  after correction for starlight dilution. The dashed lines show the power-law fit to the continuum in the optical (0.45–1  $\mu\text{m}$ ) and near-infrared (1.2–2.2  $\mu\text{m}$ ) regions. The open circles with error bars are the broadband polarimetry of Bailey et al. (1988). All spectra are shown in the rest system. Many emission lines are shown in  $F_\lambda$ , and some permitted lines (such as  $\text{H}\alpha$ ,  $\text{He I}$ ,  $\text{Pa}\beta$ ) are also shown in  $P \times F_\lambda$ .

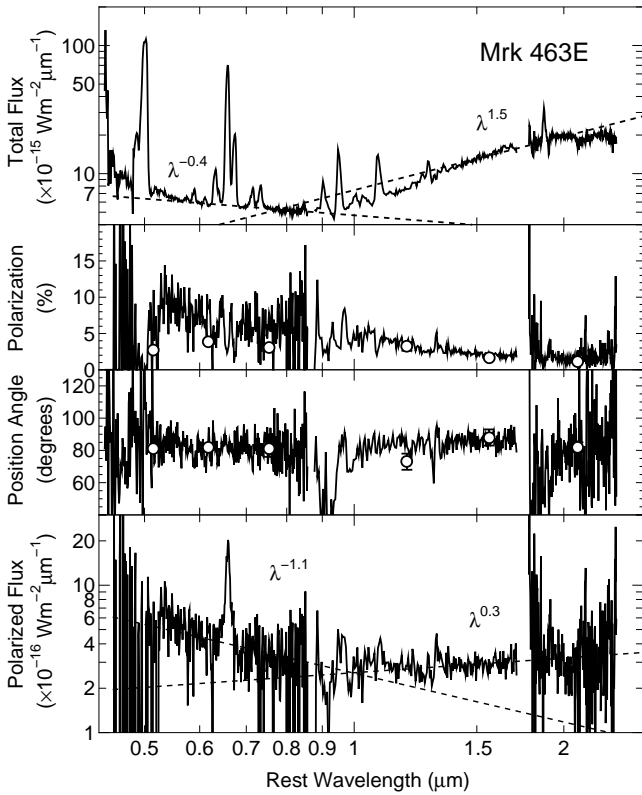


FIG. 2.—Spectropolarimetry of Mrk 463E after correction for the Galactic interstellar reddening and polarization, arranged as in Fig. 1. The dashed lines show the power-law fit to the continuum in the optical (0.45–1  $\mu\text{m}$ ) and near-infrared (1.2–2.2  $\mu\text{m}$ ) regions. The open circles with error bars are the broadband polarimetry by Young et al. (1996b).

For NGC 1068, Mrk 463E, and Mrk 1210, the results of the broadband polarimetry by Bailey et al. (1988) and Young et al. (1996b) are also shown in the figures. Our observed degrees of polarization and P.A.s agree well with their results. The degrees of polarization are slightly higher than their results, which is expected for our smaller aperture ( $0''.88 \times 2''.0$ – $3''.5$ ) than theirs ( $4''.5\phi$ : Bailey et al. 1988;  $5''.\phi$ : Young et al. 1996b), because of the smaller dilution by the unpolarized light of the extended stellar component of the host galaxy, as described in Miller & Antonucci (1983).

### 3.1. Slopes of Continuum Spectra

To determine the spectral slope of the true nuclear continuum polarization, we corrected the total flux spectrum by subtracting the host-galaxy component. Normally, the galaxy fraction ( $f_G$ ) in the observed total flux is estimated from the strengths of the stellar absorption features (such as Mg I  $b$ , Fe I) in the total flux spectrum (Miller & Antonucci 1983; Antonucci & Miller 1985; Miller & Goodrich 1990; Kay 1994; Tran et al. 1992; Tran 1995a). However, our low-resolution spectra do not resolve such features. Therefore, we fixed  $f_G$  so that the corrected degree of continuum polarization is equal to that obtained by Tran (1995a), around 0.51–0.62  $\mu\text{m}$ , after the subtraction of the host-galaxy component. The corrected degree of polarization  $P_{\text{cor}}$  was derived from

$$P_{\text{cor}} = P \frac{1}{1 - f_G(\lambda)},$$

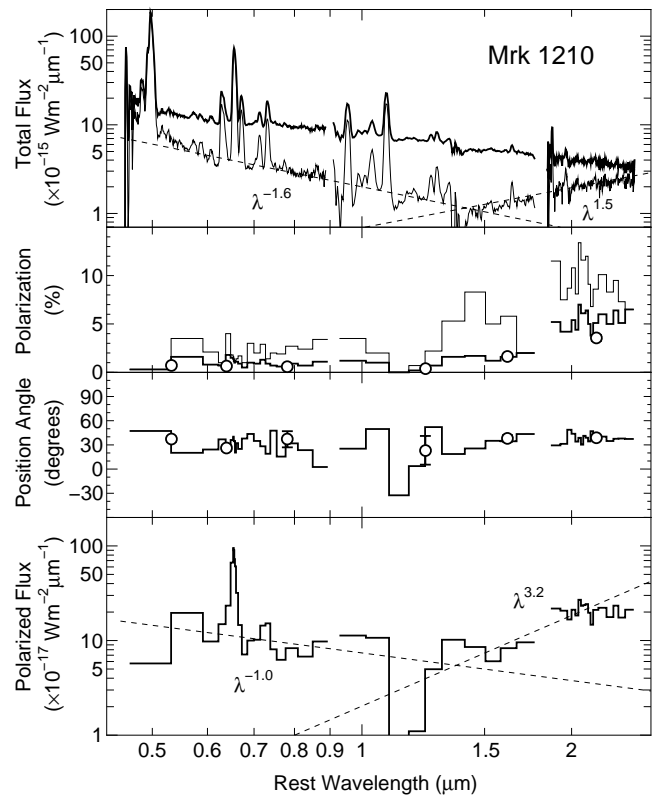


FIG. 3.—Spectropolarimetry of Mrk 1210 after correction for the Galactic interstellar reddening and polarization (thick solid curves), arranged as in Fig. 1, but with a polarization error per bin of 0.3% and 1% in the ranges 0.46–1.80 and 1.88–2.5  $\mu\text{m}$ , respectively. The thin solid curves in the top two panels show  $F_\lambda$  and  $P$  after correction for starlight dilution. The dashed lines show the power-law fit to the continuum in the optical (0.45–1  $\mu\text{m}$ ) and near-infrared (1.2–2.2  $\mu\text{m}$ ) regions. The open circles with error bars are the broadband polarimetry by Young et al. (1996b).

where  $P$  is the degree of polarization after correction for the interstellar polarization. For Mrk 436E, no subtraction ( $f_G = 0$ ) was applied, because we observed a slightly higher degree of polarization than the corrected one obtained by Tran (1995a). Tran found a small  $f_G$  of 0.25 in his  $2''.4 \times 6''$ – $7''$  aperture, and Miller & Goodrich (1990) applied  $f_G = 0$  because no stellar absorption features were visible in their spectrum. Tran also found that the spectra of elliptical galaxies fit that of the components of the host galaxies of Mrk 463E, NGC 1068, and Mrk 1210. Therefore, we adopted the composite spectrum of elliptical galaxies obtained by Mannucci et al. (2001) as the template spectrum of the host galaxies. This composite spectrum covers the range 0.1–2.4  $\mu\text{m}$ , and the region of 2.4–2.5  $\mu\text{m}$  was covered by using the intrinsic color of elliptical galaxies compiled by McAlary & Rieke (1988). The template spectrum was convolved to match our spectral resolutions and was normalized at 0.55  $\mu\text{m}$ . We show the adopted values of  $f_G$  at 0.55  $\mu\text{m}$  in Table 3 and the corrected total flux and the degree of polarization in Figures 1–3.

The spectral indices  $\beta$  of the corrected total flux  $F_\lambda$  spectra in the optical and near-infrared regions are shown in Table 3. The indices of the observed polarized flux  $P \times F_\lambda$  spectra are also shown in the table. These indices were obtained by fitting the slopes of the flux spectra with a power law  $F_\lambda \propto \lambda^\beta$ , in the range of 0.45–1.0 and 1.2–2.2  $\mu\text{m}$ , while masking the emission lines ( $\beta$  is related to  $\alpha$  in the

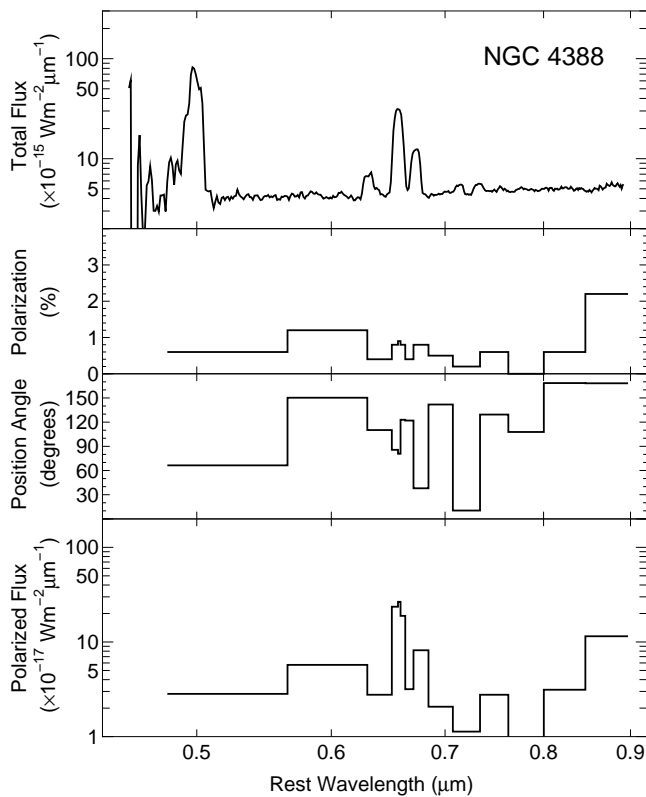


FIG. 4.—Spectropolarimetry of NGC 4388 after correction for the Galactic interstellar reddening and polarization, arranged as in Fig. 1, but with a polarization error per bin of 0.4%.

form of  $F_\nu \propto \nu^\alpha$  with  $\alpha = -\beta - 2$ ). The table also shows the spectral indices of the corrected degree of continuum polarization. They were derived by subtracting the spectral indices of the corrected total flux from those of the polarized flux [ $P = (P \times F_\lambda) / F_\lambda \propto \lambda^{\beta_P - \beta_T}$ , where  $\beta_T$  and  $\beta_P$  are the spectral indices of the corrected total and polarized fluxes].

The optical spectral index of the polarized flux basically agrees with that of the corrected total flux for all the three nuclei. That is, the corrected degree of continuum polarization is almost constant over 0.5–1  $\mu\text{m}$  in these nuclei. This is consistent with the previous suggestion that electron scattering dominates the optical continuum polarization of these nuclei.

We also compare the optical spectral indices with that of a typical type 1 nucleus. Vanden Berk et al. (2001) derived

$\beta \sim -1.6$  ( $\alpha \sim -0.4$ ) in the range 0.13–0.5  $\mu\text{m}$  from the composite spectrum of quasars and Seyfert galaxies from the Sloan Digital Sky Survey (SDSS), as opposed to other composites from, e.g., the Large Bright Quasar Survey (LBQS; Francis et al. 1991). Although they derived  $\beta \sim 0.5$  ( $\alpha \sim -2.5$ ) longward of 0.5  $\mu\text{m}$ , they found that this change in slope can be accounted for partly by contamination from the host galaxies at low redshift. Therefore,  $\beta \sim 0.5$  is unlikely to represent the true slope of the continuum of a typical type 1 nucleus longward of 0.5  $\mu\text{m}$ . If the continuum with  $\beta \sim -1.6$  continues into the range 0.5–1  $\mu\text{m}$ , our measured  $\beta$  of the polarized flux agrees with this value. As mentioned by Tran (1995b), this agreement is again consistent with the domination of electron scattering for the optical nuclear continuum polarization, because electron scattering produce a polarized flux spectrum with the same shape as the incident spectrum, assumed to be the spectrum of a type 1 nucleus. It should be noted that dust scattering can also mimic this effect over a limited range of wavelength (see § 4.4). We note that Tran (1995b) found that the mean spectral index of the polarized flux of type 2 Seyfert nuclei is  $\beta = -1.6$  in the range of 0.34–0.74  $\mu\text{m}$ . Our measured value of  $\beta$  agrees with Tran’s value.

In contrast, the near-infrared spectral index of the polarized flux differs from that of the corrected total flux for all three nuclei. That is, the corrected degree of continuum polarization is not constant for 1.0–2.2  $\mu\text{m}$  in these nuclei. In addition, it varies in wavelength with a different slope for each nucleus. The nonflatness of the corrected degree of continuum polarization indicates that a different mechanism from electron scattering is responsible for the near-infrared continuum polarization of these nuclei, such as dichroic absorption, as proposed by Young et al. (1995) for NGC 1068.

The spectral index of a typical type 1 Seyfert is  $\beta \sim 0$  ( $\alpha \sim -2$ ; Fadda et al. 1998) in the range 1.25–2.2  $\mu\text{m}$ . The measured spectral indices of the polarized flux are larger (redder) than  $\beta \sim 0$  for Mrk 1210 and NGC 1068. Those of the corrected total flux are also larger than  $\beta \sim 0$  for all the three nuclei. These reddened flux spectra again indicate a different polarization mechanism from electron scattering.

### 3.2. NGC 1068

The spectropolarimetry of NGC 1068 is shown in Figure 1. As described below, the polarization features essentially agree with the ones found by many previous authors (Angel et al. 1976; Miller & Antonucci 1983; McLean et al. 1983;

TABLE 3  
SPECTRAL INDEX

OBJECT	$f_G^c$	TOTAL FLUX <sup>a</sup>		POLARIZED FLUX		DEGREE OF POLARIZATION <sup>b</sup>	
		Optical <sup>d</sup>	Near-Infrared <sup>e</sup>	Optical <sup>d</sup>	Near-Infrared <sup>e</sup>	Optical <sup>d</sup>	Near-Infrared <sup>e</sup>
Mrk 463E.....	0.0	$-0.4^{+0.1}_{-0.1}$	$1.5^{+0.1}_{-0.1}$	$-1.1^{+0.1}_{-0.1}$	$0.33^{+0.06}_{-0.06}$	$-0.7^{+0.2}_{-0.2}$	$-1.2^{+0.2}_{-0.2}$
Mrk 1210.....	$0.52^{+0.07}_{-0.09}$	$-1.7^{+0.4}_{-0.6}$	$1.7^{+1.8}_{-1.2}$	$-1.0^{+0.6}_{-0.6}$	$3.2^{+0.3}_{-0.3}$	$0.7^{+0.9}_{-0.7}$	$1.3^{+1.2}_{-1.8}$
NGC 1068.....	$0.70^{+0.02}_{-0.04}$	$-1.9^{+0.4}_{-0.3}$	$4.4^{+0.2}_{-0.3}$	$-1.70^{+0.04}_{-0.04}$	$2.74^{+0.01}_{-0.01}$	$0.2^{+0.3}_{-0.4}$	$-1.7^{+0.3}_{-0.2}$

NOTE.—Spectral index  $\beta$  is defined by  $F_\lambda \propto \lambda^\beta$ .

<sup>a</sup> Total flux spectrum after correction for starlight dilution.

<sup>b</sup> Derived by subtracting the spectral index of the total flux from that of the polarized flux.

<sup>c</sup> Fraction of the host-galaxy component measured at 0.55  $\mu\text{m}$ .

<sup>d</sup> Measured in the range of 0.45–1.0  $\mu\text{m}$ .

<sup>e</sup> Measured in the range of 1.2–2.2  $\mu\text{m}$ .

Antonucci & Miller 1985; Bailey et al. 1988; Miller et al. 1991; Tran 1995a, 1995b; Young et al. 1995; Inglis et al. 1995; Alexander, Young, & Hough 1999), but our spectra cover a much broader wavelength range.

In the optical, the observed degree of continuum polarization rises toward the blue, while the P.A. remains nearly constant ( $\sim 93^\circ$ ). Miller & Antonucci (1983) showed that this rise is a result of the decreasing dilution by the unpolarized stellar component toward the blue. After correction for this dilution, they found that the continuum has a constant degree of polarization ( $\sim 16\%$ ) over the UV and optical wavelengths. In addition, they showed that the P.A. is perpendicular to the radio source structure. Therefore, Antonucci & Miller (1985) proposed that electrons are located along the axis defined by this structure.

In the near-infrared, the observed degree of continuum polarization rises toward  $2 \mu\text{m}$ , while the P.A. changes smoothly to  $120^\circ$ . Young et al. (1995) pointed out that this change in P.A. is a result of a change in the main polarization mechanisms. They modeled the polarization with a combination of electron scattering and dichroic absorption by aligned grains. They proposed that dichroic absorption dominates longward of  $1.4 \mu\text{m}$ . Packham et al. (1997) found a torus extinction of  $A_V = 36$  and an efficiency of dichroic absorption ( $P_{\text{max}}/A_V$ ) of  $1.25\%$  on the basis of this model. Although a change in P.A. is often interpreted as resulting from a change in main polarization mechanism, it can also arise from a change, with wavelength, in the relative contribution from two different scattering regions. It only requires a different geometry.

To inspect our results in detail, we compare our optical spectra with those of Tran (1995b) and Young et al. (1995). They used a narrow slit of width  $2''4$  and  $1''03$ , which is slightly larger than our slit width ( $0''88$ ). In our observations, the polarized fluxes are  $9.7 \times 10^{-15}$  and  $4.7 \times 10^{-15} \text{ W m}^{-2} \mu\text{m}^{-1}$  at  $0.51$  and  $0.70 \mu\text{m}$ , respectively. The spectral index determined from these fluxes is  $\beta = -2.3$ ; this is similar to  $\beta = -2.7$  (Tran 1995b) and  $\beta = -2.5$  (Young et al. 1995), derived from the fluxes at the same wavelengths. The degrees of polarization are  $4.4\%$  at  $0.51 \mu\text{m}$  and  $2.2\%$  at  $0.70 \mu\text{m}$ , higher than those of Tran (1995b) and Young et al. (1995), as expected for our narrower slit width. The P.A.s are  $96^\circ$  at  $0.51 \mu\text{m}$  and  $90^\circ$  at  $0.70 \mu\text{m}$ , in agreement with the value of  $\sim 95^\circ$  found by Tran (1995b). However, a small rotation of the P.A., which reaches  $87^\circ$  at  $0.88 \mu\text{m}$ , was found. Miller et al. (1991) pointed out that some contribution from scattering light from the dust knot, located  $5''$  northeast of the nucleus, can produce some rotation of the P.A., because it has a different P.A. of  $125^\circ$  and because the polarized flux from it rises faster toward the blue than that from the nucleus. Although this knot is located outside our aperture, some light from the knot may be included in our aperture because of the relatively poor seeing conditions.

For the near-infrared, we compare our spectra with those of Young et al. (1995) and Alexander et al. (1999), who used slits with widths of  $3''08$  and  $1''23$ , respectively. We measured the polarized fluxes of  $2.8 \times 10^{-15}$  and  $10.5 \times 10^{-15} \text{ W m}^{-2} \mu\text{m}^{-1}$  at  $1.2$  and  $2.05 \mu\text{m}$ , respectively. The spectral index derived from these fluxes is  $\beta = 2.5$ , in agreement with  $\beta = 3.1$  derived from the fluxes in Young et al. (1995). The observed degrees of polarization and the P.A.s are also consistent with both of them, although our observed degree of polarization is slightly smaller than that of Young et al. (1995) around  $2 \mu\text{m}$ . Our observed degrees of polarization

and the P.A.s are  $1.8\%$  and  $99^\circ$  (at  $1.2 \mu\text{m}$ ),  $2.1\%$  and  $101^\circ$  (at  $1.3 \mu\text{m}$ ),  $3.6\%$  and  $115^\circ$  (at  $1.7 \mu\text{m}$ ), and  $4.3\%$  and  $120^\circ$  (at  $2.05 \mu\text{m}$ ).

We also compare the near-infrared slope of the corrected total flux spectrum with that of the nonstellar nuclear flux derived by Alonso-Herrero et al. (2001). They estimated these fluxes by the nucleus+bulge deconvolution of the observed surface brightness profiles of the near-infrared images. The spectral index derived from their estimated fluxes in the *J* and *K* bands is  $\beta = 4.8$ . This value agrees well with our estimated index,  $\beta = 4.4^{+0.2}_{-0.3}$ .

### 3.3. Mrk 463E

Mrk 463E is a type 2 nucleus in an interacting double Seyfert system, separated by about  $4''$  along the east-west direction (Hutchings & Neff 1989). Many authors have taken optical or near-infrared spectropolarimetric data of this object (Miller & Goodrich 1990; Goodrich 1992; Ruiz, Rieke, & Schmidt 1994; Kay 1994; Tran 1995b; Young et al. 1996b). Miller & Goodrich (1990) showed that its optical continuum is highly polarized ( $7.7\%$ ) and that both the degree of polarization and the P.A. rise toward the blue. They suggested that both dust and electron scattering contribute to the optical polarization and that the two mechanisms have different P.A.s. Tran (1995b) found a highly polarized knot extending  $\sim 3''$  to the north of the nucleus by optical imaging polarimetry. He noted that if this knot is a dusty region similar to that in NGC 1068, the rise in the degree of polarization and the P.A. could be explained.

Our spectropolarimetry of Mrk 463E is shown in Figure 2. We compare our optical spectra with those of Miller & Goodrich (1990) and Tran (1995b). Our observed degrees of continuum polarization rise from  $7.5\%$  at  $0.62 \mu\text{m}$  to  $10.4\%$  at  $0.54 \mu\text{m}$ . This rise agrees well with that of Miller & Goodrich (1990). They observed  $\sim 5.5\%$  at  $0.62 \mu\text{m}$  and  $\sim 8\%$  at  $0.54 \mu\text{m}$  in the rest frame. However, our slope of the polarized flux spectrum seems to be bluer than those of both Miller & Goodrich (1990) and Tran (1995b). Our observed polarized fluxes are  $6.5 \times 10^{-16}$  and  $3.6 \times 10^{-16} \text{ W m}^{-2} \mu\text{m}^{-1}$  at  $0.54$  and  $0.70 \mu\text{m}$ , respectively. Although these fluxes produce  $\beta = -2.3$ , their polarized flux spectra are flatter ( $\beta \sim -1$ ) in this wavelength range. The averaged value of the P.A. over  $0.54$ – $0.62 \mu\text{m}$  is  $82^\circ$ , and the small rise in the P.A. ( $<10^\circ$  over  $0.37$ – $0.69 \mu\text{m}$ ) found by Miller & Goodrich (1990) is unclear in our spectrum because of the poor S/N ratio. Kay (1994) and Tran (1995b) noted that this P.A. is nearly perpendicular to the scattering cone (Tremonti et al. 1996), referred to by Uomoto et al. (1993) as an “optical jet.”

In the near-infrared, Mrk 463E shows no rise in the degree of polarization and no change in the P.A. toward the longer wavelength, unlike NGC 1068 and Mrk 1210. The polarized flux spectrum is almost flat ( $\beta = 0.33 \pm 0.06$ ), although the corrected total flux spectrum shows a rise toward the longer wavelength with  $\beta = 1.5 \pm 0.1$ . This corresponds to the decrease in the corrected degree of polarization with  $\beta = -1.2 \pm 0.2$  toward the longer wavelength. The flatness of the polarized flux spectrum agrees with  $\beta = -0.4 \pm 0.4$  derived from the broadband polarimetry of Young et al. (1996b). Young et al. modeled the optical to near-infrared polarization with a combination of electron scattering and dichroic absorption by aligned grains in an obscuring torus. They found a torus extinction of

$A_V = 17.5$  and an efficiency of dichroic absorption,  $P_{\max}/A_V = 0.27\%$ , which is lower in Mrk 463E than in NGC 1068.

#### 3.4. Mrk 1210

Our spectropolarimetry of Mrk 1210 is shown in Figure 3. The optical observed degree of polarization is small ( $\sim 1.0\%$  in  $0.46\text{--}0.89\ \mu\text{m}$ ), unlike NGC 1068 and Mrk 463E. On the other hand, in the near-infrared, like NGC 1068, the observed degree of polarization rises toward longer wavelength, reaching  $\sim 5.0\%$  at  $2.15\ \mu\text{m}$ . Although the P.A. remains almost constant over the optical and near-infrared, it seems to rotate slightly from  $30^\circ$  in the optical ( $0.46\text{--}0.89\ \mu\text{m}$ ) to  $38^\circ$  in the  $2\ \mu\text{m}$  region ( $1.85\text{--}2.46\ \mu\text{m}$ ).

Tran et al. (1992) and Tran (1995b) presented nuclear optical spectropolarimetry. Their observed polarization is  $0.8\%\text{--}1.1\%$  at a P.A. of  $28^\circ\text{--}29^\circ$ , in the range of  $0.4\text{--}0.7\ \mu\text{m}$ . Our observed polarization agrees with their results. Although Tran (1995b) reported a rise in the observed degree of optical continuum polarization to the blue, we do not see this rise in our spectrum. This is likely to be the result of the lower amount of starlight dilution in our spectrum due to the smaller aperture used. They showed that after correction for starlight dilution, the degree of continuum polarization is almost flat ( $\sim 4\%$ ) over the optical. Our measured spectral index for the corrected degree of continuum polarization ( $\beta = 0.7^{+0.9}_{-0.7}$ ) basically agrees, although our slope tends to be somewhat redder. As suggested by Tran (1995b), this flatness indicates that electron scattering dominates the optical continuum polarization of the nucleus of Mrk 1210. The spectral index of the polarized flux is  $\beta = -1.0 \pm 0.6$ , agreeing with  $\beta = -0.7$  obtained by Tran (1995b).

The near-infrared spectral index of the polarized flux is  $\beta = 3.2 \pm 0.3$ . This agrees with  $\beta = 2.4 \pm 1.0$  derived from the broadband polarimetry of Young et al. (1996b) and is very similar to that of NGC 1068. It may indicate that the same mechanism (dichroic absorption by aligned grains) works on the near-infrared continuum polarization in both NGC 1068 and Mrk 1210. However, the near-infrared spectral indices of the degree of polarization for both nuclei are rather different. This could indicate the existence of an additional unpolarized component in Mrk 1210, electron scattering light, as described below (§ 4.5).

#### 3.5. NGC 4388

Our spectropolarimetry of NGC 4388 is shown in Figure 4. The averaged continuum polarization over  $0.51\text{--}0.62\ \mu\text{m}$  is  $2.0\% \pm 0.5\%$  with the P.A.  $68^\circ \pm 7^\circ$ . Kay (1994), in an aperture of  $2'' \times 5''\text{--}7''$ , measured a degree of polarization of  $0.44\% \pm 0.35\%$  and P.A. of  $105^\circ \pm 19^\circ$  in the range of  $0.415\text{--}0.465\ \mu\text{m}$ , after correction for the interstellar polarization. She also found that after correction for starlight dilution, the degree of polarization is  $2.0\% \pm 2.1\%$  and the P.A. is  $93^\circ \pm 29^\circ$ . Our observed polarization agrees better with his corrected values, which is expected for our smaller aperture.

### 4. POLARIZATION MODELS

To model the spectral slopes of the continuum polarization of type 2 Seyfert nuclei, we consider the polarizations from the four following components: (1) electron scattering

in ionization cones aligned along the polar axis, (2) dust scattering in dusty regions in the cones, (3) dichroic absorption by aligned dust grains in an obscuring torus, (4) dust scattering in the torus. For simplification, we calculate these polarizations separately as described below. In this paper, we assume an isotropic point source as the central radiative source. The flux spectra of the models presented in this section are normalized to the flux spectrum of the radiative source.

We note a recent Monte Carlo investigation of dust scattering in *IRAS*-selected AGNs based on the UV and optical spectropolarimetry by Hines et al. (2001). They considered a dusty sphere of modest optical depth ( $\tau_V = 0.25\text{--}4.0$ ) illuminated axisymmetrically from within by a power-law QSO spectrum. Manzini & di Serego Alighieri (1996) also modeled dust scattering and UV and optical polarization in radio galaxies with various grain size distributions.

#### 4.1. The Monte Carlo Code

To calculate the polarization from scattering by electrons or dust grains, we developed a Monte Carlo radiative transfer code. It is based on the descriptions of Witt (1977), Fischer, Henning, & Yorke (1994), and Code & Whitney (1995). In the Monte Carlo method the radiation is partitioned into many “weighted” photons. Each weighted photon is traced until it exits from the scattering medium or it is absorbed. At each scattering point, its weight, Stokes parameters, and direction of propagation are changed. For scattering by an electron or a spherical dust grain, using the scattering matrix, the new Stokes parameters ( $I, Q, U, V$ )<sub>*i*</sub> and weight  $W_i$  for the *i*th scattering are calculated by

$$\begin{pmatrix} I \\ Q \\ U \\ V \end{pmatrix}_i = \begin{pmatrix} P_1 & P_2 & 0 & 0 \\ P_2 & P_1 & 0 & 0 \\ 0 & 0 & P_3 & -P_4 \\ 0 & 0 & P_4 & P_3 \end{pmatrix} \begin{pmatrix} I \\ Q \\ U \\ V \end{pmatrix}_{i-1},$$

$$W_i = \omega W_{i-1},$$

where ( $I, Q, V, U$ )<sub>*i*</sub> and ( $I, Q, V, U$ )<sub>*i-1*</sub> have to be measured with reference to the scattering plane, the elements  $P_j$  ( $j = 1, \dots, 4$ ) are functions of the scattering angle, and  $\omega$  is the albedo for single-scattering ( $\omega = 1$  for electrons). After each scattering, ( $I, Q, U, V$ )<sub>*i*</sub> are normalized with the intensity  $I$ .

In the Monte Carlo method, quantities such as the initial direction of each photon and the scattering angles are determined from probability distributions using random numbers. In this paper, the initial direction is limited to the direction toward the scattering medium but is distributed uniformly within it so that the radiation is isotropic. The polar and azimuth angle of scattering are calculated in the same way as Bianchi, Ferrara, & Giovanardi (1996).

When a photon exits from the scattering medium, its Stokes parameters are summed into arrays binned in the exiting direction. Before summing, these are scaled with its weight. In this paper, we assume an axisymmetric distribution of scatterers around the nucleus, requiring binning only in the polar angle. Finally, the Stokes parameters are normalized with the number of the total incident photons, which is on the order of  $10^7$ .

To test our code, we calculated the polarization from dust scattering within the spherical blob described in Code & Whitney (1995). Our results agreed well.

#### 4.2. Scattering Properties of the Dust

For dust scattering we adopted the dust model of Draine & Lee (1984) and Mathis, Rumpl, & Nordsieck (1977) for the Galactic diffuse interstellar medium. The model consists of graphite and silicate spherical grains with a power-law size distribution as

$$dn_i = A_i n_H a^{-3.5} da \quad (a_{\min} < a < a_{\max}),$$

where  $dn_i$  is the number density of grains of composition  $i$  with radii in the interval  $[a, a + da]$ ,  $n_H$  is the number density of H nuclei, and  $A_i$  is the abundance of grains of composition  $i$ . The upper and lower limits are  $a_{\min} = 0.005 \mu\text{m}$  and  $a_{\max} = 0.25 \mu\text{m}$ .

The extinction and scattering cross sections  $C_{\text{ext}}$  and  $C_{\text{sca}}$ , and the elements of the scattering matrix  $P_j(\theta)$  ( $j = 1, \dots, 4$ ) are given by

$$C_{\text{ext}} = \sum_i \int_{a_{\min}}^{a_{\max}} \pi a^2 \left[ Q_{\text{ext}}^i(a) \frac{dn_i}{da} a \right] d \ln a,$$

$$C_{\text{sca}} = \sum_i \int_{a_{\min}}^{a_{\max}} \pi a^2 \left[ Q_{\text{sca}}^i(a) \frac{dn_i}{da} a \right] d \ln a,$$

$$P_j(\theta) = \sum_i \int_{a_{\min}}^{a_{\max}} \left[ P_j^i(\theta, a) \frac{dn_i}{da} a \right] d \ln a \quad (j = 1, \dots, 4),$$

where  $Q_{\text{ext}}^i(a)$ ,  $Q_{\text{sca}}^i(a)$ , and  $P_j^i(\theta, a)$  are the extinction and scattering efficiency factors and the elements of scattering matrix, respectively, of grains of composition  $i$  with radius  $a$ . Values of  $Q_{\text{ext}}^i(a)$ ,  $Q_{\text{sca}}^i(a)$ , and  $P_j^i(\theta, a)$  were calculated using a Mie scattering code derived from BHMIE in Bhorén & Huffman (1983). We adopted the dielectric functions and the abundances given by Draine & Lee (1984) and Draine (1985). Therefore,  $C_{\text{ext}}$ ,  $C_{\text{sca}}$ , and the albedo  $\omega = C_{\text{sca}}/C_{\text{ext}}$  are identical with their results.  $P_j(\theta)$  are similar to the results by White (1979), who used similar dielectric functions for a graphite and olivine grain mixture.

The degree of linear polarization from scattering of unpolarized incident light is represented by  $P_2/P_1$ . White (1979) found that for the Mathis et al. (1977) grain mixture  $P_2/P_1$  can be approximately described by a scaled Rayleigh-like function plus a bump of the form

$$P_2/P_1 \approx -p_l \frac{1 - \cos^2 \theta}{1 + \cos^2 \theta} + B_l(\theta, b_l),$$

$$B_l(\theta, b_l) = \begin{cases} b_l(1 - |\theta - 145^\circ|/35^\circ) & |\theta - 145^\circ| < 35^\circ, \\ 0 & |\theta - 145^\circ| \geq 35^\circ, \end{cases}$$

where  $p_l$  is the peak linear polarization and  $b_l$  is the size of the bump. Figure 5 shows the variations of  $p_l$  and  $b_l$  in wavelength, determined by the least-squares fitting of our  $P_2/P_1$  to this form. The results for  $\lambda < 1 \mu\text{m}$  are in good agreement with those of White (1979). The peak polarization  $p_l$  is rather flat around  $0.3\text{--}0.7 \mu\text{m}$  and rises steeply toward the longer wavelength between  $0.7$  and  $1.4 \mu\text{m}$ . For wavelength longer than  $1.4 \mu\text{m}$ , it approaches the case for Rayleigh scattering.

The variation of  $P_2/P_1$  depends mainly on  $p_l$ , because the bump is small. In addition, the wavelength dependence of

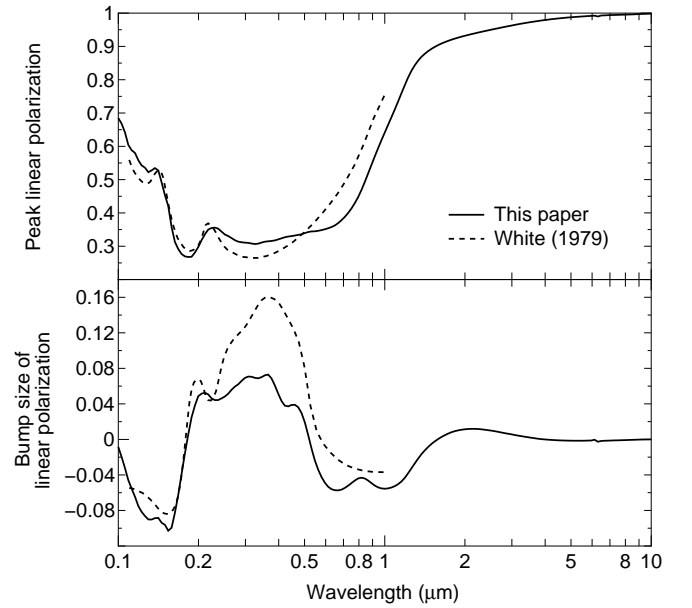


FIG. 5.—Peak linear polarization (*top*) and bump size of linear polarization (*bottom*) vs. wavelength for dust mixtures with the MRN size distribution. The solid line is the graphite and astronomical silicate grains mixture of Draine & Lee (1984). The dashed line presents the results by White (1979) of graphite and olivine grains mixture.

the degree of polarization for such single-scattering systems is independent of the geometry and depends only on  $P_2/P_1$ . Therefore, it is expected that the degree of polarization from a dusty region rises with a similar slope to that of  $p_l$  in our observed wavelength range, at least when the optical depth of the region is so low that single-scattering dominates.

#### 4.3. Electron Scattering in Cones

Scattering in conical electron clouds has been successful in modeling the optical polarization for NGC 1068 (Miller et al. 1991; Young et al. 1995; Packham et al. 1997) and for other type 2 AGNs (Young et al. 1996b). These cones are defined by five parameters: the inner radius  $r_{c1}$ , the outer radius  $r_{c2}$ , the half-opening angle  $\theta_c$ , the optical depth along polar axis  $\tau_c$ , and the power-law index  $\alpha_c$  for the radial density dependence of electrons [ $n_c(r) \propto r^{-\alpha_c}$ , where  $n_c(r)$  is the electron density at the distance  $r$  from the nucleus]. The geometry of the cones is shown in Figure 6a. In this paper we assume  $r_{c1} = 30 \text{ pc}$  and  $\theta_c = 30^\circ$ , similar to the values found by Miller et al. (1991) and Packham et al. (1997) for NGC 1068. We also assume  $r_{c2} = 10r_{c1}$  and  $\alpha_c = 2$ , following Miller et al. (1991).

Figure 7 shows the calculated polarization for electron scattering in the cones with  $\tau_c = 0.01, 0.03, 0.1, 0.3, 0.1, 1,$  and  $3$ . The plane of polarization is perpendicular to the polar axis of the cones. The degree of polarization is similar to the result of Wolf & Henning (1999), who calculated the polarization for multiple scattering in similar cones. At  $\tau_c < 1$ , the fluxes and the variations with inclination agree with the analytic solution for single-scattering (e.g., Brown & McLean 1977). At  $\tau_c \geq 1$ , the fluxes are smaller than this solution. The scattered and polarized fluxes at  $\tau_c = 1$  are only 68% and 61% of those expected from the solution for single-scattering, respectively. However, the effect of multiple scattering in the cones of Seyfert galaxies is negligible,

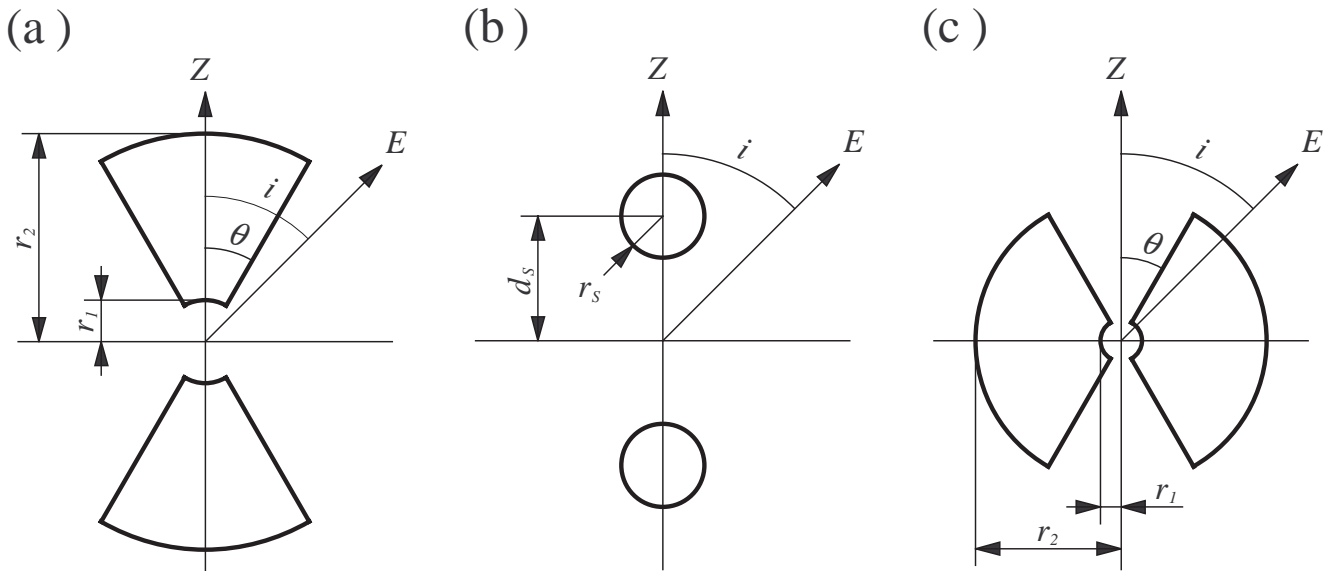


FIG. 6.—Geometries for scattering in (a) electron cones, (b) dusty spheres along the polar axis, and (c) a flared disk representing a dusty torus.  $Z$  is the polar axis of the system, and  $E$  is the direction to the observer.

because a small  $\tau_c$  is expected (e.g., Miller et al. [1991] found  $\tau_c = 0.04$  for NGC 1068).

#### 4.4. Dust Scattering in Cones

From near-infrared imaging polarimetry and the modeling of NGC 1068, Packham et al. (1997) calculated the radius of the dusty region, found by Miller et al. (1991), to be 194 pc, assuming a spherical cloud. To model such dusty regions, we assume a dusty sphere placed at each side of the equatorial plane of the nucleus along the polar axis, as shown in Figure 6b. These spheres are defined by three parameters: the radius  $r_s$ , the distance from the nucleus at the centers  $d_s$ , and the optical depth along the polar axis  $\tau_s$ , which is measured at  $0.55 \mu\text{m}$ . In this paper, we fix  $r_s = 100$  pc and  $d_s = 300$  pc, similar to the values in the models of Packham et al. (1997) and Inglis et al. (1995) for NGC 1068. We calculate the polarization for  $\tau_s = 0.1, 0.3, 1, 3, 10$ , and 30 at 11 wavelengths between  $0.45$  and  $2.5 \mu\text{m}$ .

Packham et al. (1997) assumed that the number density of dust grains within the spheres varies as  $n_s(r) \propto r^{-\alpha_s}$ , where  $r$  is the distance from the nucleus and  $\alpha_s$  is the power-law index for the radial number density. They found that  $\alpha_s = 1$  fits their observations. However, we found only small differences in our calculated results for  $\alpha_s = 0, 1$ , and 2. This is because as  $d_s$  is larger than  $r_s$ , there is no large difference in densities between the nucleus and nonnucleus side of the sphere and because we do not take into account the spatial profile of the flux. Therefore, we present below only the result for  $\alpha_s = 0$  (uniform density distribution).

Figures 8a and 8b show the scattered and polarized fluxes and the degree of polarization from the dusty spheres as a function of inclination. The plane of polarization is perpendicular to the polar axis of the nucleus. These results are similar to the results of Code & Whitney (1995) for a dusty blob. At  $\tau_s \leq 1$ , the scattered and polarized fluxes increase proportionally with  $\tau_s$ , or the number of scatterers. For the optical ( $0.55 \mu\text{m}$ ), at  $\tau_s > 1$ , neither of the fluxes increase proportionally with  $\tau_s$  any more, and then they decrease at

$\tau_s > 3$ , because of the absorption inside the dusty spheres. For the near-infrared ( $2.15 \mu\text{m}$ ), the fluxes increase proportionally with  $\tau_s$ , for  $\tau_s \leq 10$ . This difference is, of course, due to the much lower extinction in the near-infrared than that in the optical,  $\tau_{0.55}/\tau_{2.15} = 11$  (Draine & Lee 1984). For  $0.55 \mu\text{m}$ , at  $\tau_s < 1$ , the scattered fluxes show large increases as the inclination decreases, relative to the case of the electron cones. This is due to the predominance of forward scattering for dust grains. However, at  $\tau_s > 1$ , the scattered flux is almost independent of the inclination, while the polarized flux varies much more steeply with inclination. The degree of polarization decreases as  $\tau_s$  increases, approaching the limit where scattering occurs on the surface, and increasing  $\tau_s$  has little effect on the results (Code & Whitney 1995). The maximum degree of polarization at an inclination of  $90^\circ$  decreases from 29% at  $\tau_s = 0.1$  to 21% at  $\tau_s = 10$ .

Figures 9a and 9b show the scattered and polarized flux spectra and the degree of polarization of the dusty spheres with various  $\tau_s$ . At  $\tau_s < 1$ , the scattered and polarized flux spectra rise toward the blue. However, at  $\tau_s > 1$ , the slope of both spectra is flatter and the flux spectra even rises toward the red for  $\lambda \lesssim 1-1.5 \mu\text{m}$ . These increments of the slope are somewhat larger at the inclination  $34^\circ$  than at  $89^\circ$ . In contrast, the wavelength dependence of the degrees of polarization is almost independent of  $\tau_s$ , although the absolute values decrease with  $\tau_s$  and with decreasing inclination. The variation is similar to that of the peak polarization of a single scatterer (Fig. 5), as expected.

Figures 10a and 10b show the spectral indices of the scattered flux and the degree of polarization as a function of  $\tau_s$ . It is clear that the spectral index of the spectrum of the degree of polarization is almost constant, even at high  $\tau_s$ . Its value is  $\sim 1$  in the optical and  $\sim 0.3$  in the near-infrared. It is also insensitive to the inclination except for high  $\tau_s$  in the near-infrared.

In the optical, the spectral indices of the corrected degrees of polarization for NGC 1068 and Mrk 463E, are much flatter than expected for scattering from dusty spheres but are not consistent with the flat spectrum expected for electron

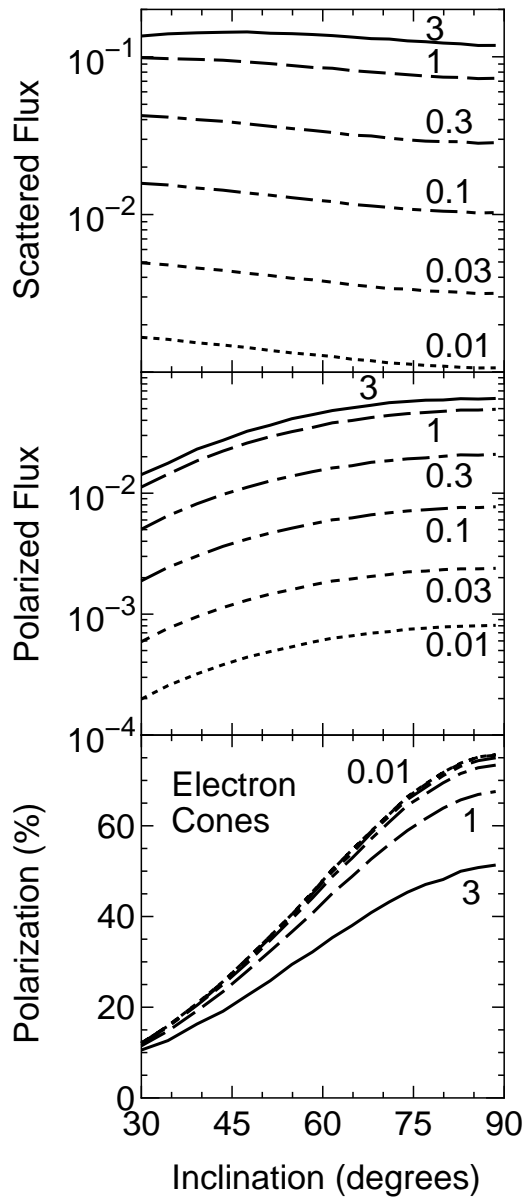


FIG. 7.—Model polarization for scattering in electron cones with various optical depths, as a function of inclination angle. From top to bottom are the scattered and polarized fluxes and the degree of polarization. The fluxes are normalized with the flux of a nucleus. Each panel shows lines for six optical depths of the cones (0.01: dotted line; 0.03: short-dashed line; 0.1: double-dotted-dashed line; 0.3: dot-dashed line; 1: long-dashed line; and 3: solid line). The parameters of the cones are the inner radius of 30 pc, the outer radius of 300 pc, the half opening angle of  $30^\circ$ , and the power-law index of 2 for the radial density distribution.

scattering. The degree of polarization for both electron and dust scattering ( $P'_\lambda$ ) is given by

$$P'_\lambda = \frac{P_e F_e + P_d F_d \lambda^{\beta_p}}{F_e + F_d \lambda^{\beta_s}},$$

where  $F_e$  and  $F_d$  are the scattered flux (measured at  $1 \mu\text{m}$ ) from electron and dust scattering respectively,  $P_e$  and  $P_d$  are the degrees of polarization in the scattered fluxes, and  $\beta_s$  and  $\beta_p$  are the spectral index of the scattered and polarized fluxes from the dusty spheres, respectively ( $\beta_s = -1.8$ – $0.6$  and  $\beta_p = -0.8$ – $1.6$ ; Fig. 10). The possible value of the spectral index of  $P'_\lambda$  is  $\beta' = -0.8$ – $1.8$ . The minimum value of  $\beta'$

occurs at  $F_e \gg F_d \lambda^{\beta_s}$  and  $P_e F_e \ll P_d F_d \lambda^{\beta_p}$ , namely, when the light from electron scattering dominates the total flux and the polarized flux is negligible. The maximum value of  $\beta'$  occurs at  $F_e \ll F_d \lambda^{\beta_s}$  and  $P_e F_e \gg P_d F_d \lambda^{\beta_p}$ , namely, when the light from dust scattering dominates the total flux and the polarized flux is negligible.

The spectral index for NGC 1068 ( $\beta = 0.2$ ) is in the range of possible indices for a combination of electron and a small amount of dust scattering. This is consistent with the previous suggestion that the small rotation of P.A. is due to a small contribution of dust scattering with a different P.A. from that of electron scattering. The index for Mrk 463E ( $\beta = -0.7$ ), together with a redder polarized flux spectrum than for a typical type 1 nucleus, indicates that dust scattering contributes significantly for this object. The negative value of  $\beta$  requires that electron scattering dominates the total flux spectrum, but dust scattering dominates the polarized flux spectrum. The redder spectrum of the total flux relative to that of a typical type 1 nucleus is inconsistent with this requirement, because electron scattering does not redden the spectrum. However, this reddening might be due to residual light from the red spectrum of the host galaxy, because we have not corrected for starlight dilution for this nucleus. For Mrk 1210, the index ( $\beta = 0.7$ ) is similar to that of dusty spheres, suggesting that dust scattering contributes greatly to both the total and polarized fluxes. If dust scattering does dominate, then  $\tau_s = 3$ – $10$ , because the spectral index of the corrected total flux becomes  $\beta \sim 0$  by normalizing with the index of a typical type 1 nucleus ( $\beta \sim -1.6$ ), as assumed for the incident flux (Fig. 10a).

In the near-infrared, the spectral indices of the corrected degree of polarization of all three nuclei are very different from that of the dusty spheres. Therefore, dust scattering alone is unlikely to be the dominant mechanism in the near-infrared continuum polarization of these nuclei. A combination with electron scattering is also unlikely for these nuclei, although this combination could produce a range of  $\beta' = -2.9$ – $3.2$ . This is because the corrected total and polarized fluxes of these nuclei rise toward the longer wavelength in the near-infrared, while those of the dusty spheres rise toward the shorter wavelength or remain constant at these wavelengths.

#### 4.5. Dichroic Absorption in Torus

The normalized emergent and polarized fluxes through a torus are described as  $e^{-\tau_\lambda}$  and  $P_\lambda e^{-\tau_\lambda}$ , respectively, where  $\tau_\lambda$  is the optical depth of the torus along our line of sight to the central source, and  $P_\lambda$  is the degree of polarization produced by aligned grains in the torus, at the wavelength  $\lambda$ . The spectral indices of these fluxes can be simply described by  $\tau_t$ , where  $\tau_t$  is  $\tau_\lambda$  at  $0.55 \mu\text{m}$ . Here we consider only the near-infrared polarization, because the emergent and polarized fluxes through the torus are negligible in the optical region with the high optical depths ( $\tau_t \gtrsim 10$ ) expected for type 2 Seyfert nuclei, as mentioned in § 1. Assuming the near-infrared Galactic interstellar extinction and polarization curves have the form  $\tau_\lambda \propto \lambda^{-1.8}$  and  $P_\lambda \propto \lambda^{-1.8 \pm 0.2}$  (Nagata 1990; Martin & Whittet 1990; Martin et al. 1992; Nagata, Kobayashi, & Sato 1994), the spectral indices in the range of  $1.25$ – $2.15 \mu\text{m}$  are represented by

$$\beta = \begin{cases} 0.26\tau_t & \text{for emergent flux,} \\ 0.26\tau_t - (1.8 \pm 0.2) & \text{for polarized flux.} \end{cases}$$

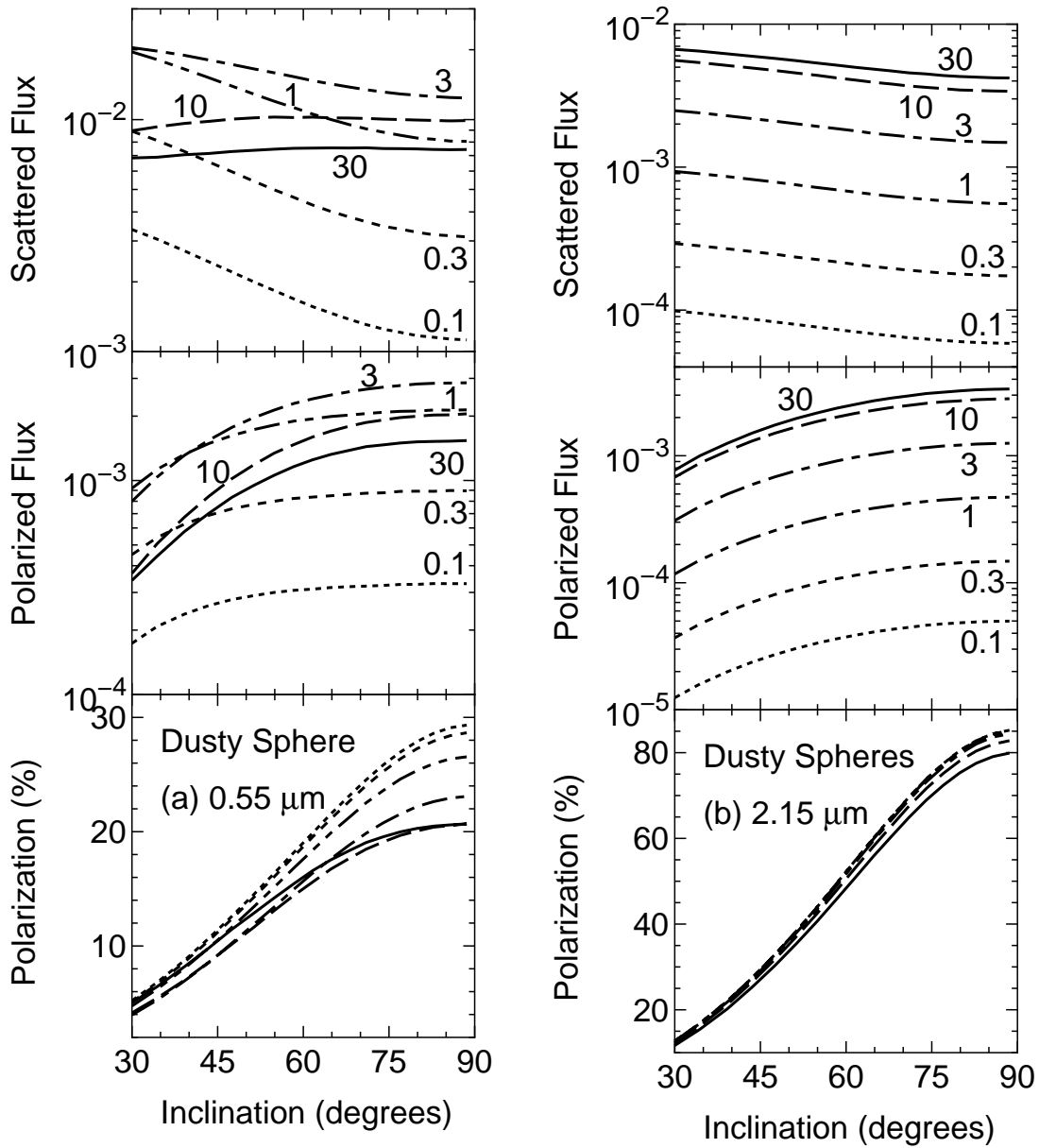


FIG. 8.—Model polarization for scattering in dusty spheres with various optical depths, as a function of inclination. The polarization at (a)  $\lambda = 0.55$  and (b)  $2.15 \mu\text{m}$  are shown. From top to bottom are the scattered and polarized fluxes and the degree of polarization. The fluxes are normalized with the flux of a nucleus. Each panel shows lines for six optical depths of the dusty sphere at  $0.55 \mu\text{m}$  (0.1: dotted line; 0.3: short-dashed line; 1: double-dotted-dashed line; 3: dot-dashed line; 10: long-dashed line; and 30: solid line).

Here the factor 0.26 between the two wavelengths 1.25 and  $2.15 \mu\text{m}$  was derived from

$$\frac{(\tau_\lambda/\tau_t)_1 - (\tau_\lambda/\tau_t)_2}{\ln(\lambda_2/\lambda_1)}.$$

The near-infrared spectral index of the corrected degree of polarization of NGC 1068 ( $\beta = -1.7^{+0.3}_{-0.2}$ ) agrees well with that of dichroic absorption. If we assume that dichroic absorption dominates for this nucleus and also that the central source has the same spectral index as a typical type 1 Seyfert nucleus ( $\beta = 0$ ; Fadda et al. 1998), then  $\tau_t = 17 \pm 1$  is derived from the spectral index of the polarized flux ( $\beta = 2.7$ ). This  $\tau_t$  agrees with the previous estimations derived by using similar methods ( $\tau_t = 18$ – $23$ : Bailey et al. 1988;  $\tau_t \sim 41$ : Young et al. 1995;  $\tau_t \sim 32$ : Packham et al.

1997;  $\tau_t = 16 \pm 6$ : Lumsden et al. 1999). From the corrected degree of polarization of  $P_K = 5.0\%$  at  $2.15 \mu\text{m}$ , the polarization efficiency,  $P_K/\tau_K = 2.5\%$ , using  $\tau_K/\tau_V = 0.12$  (Cardelli et al. 1989), or  $P_V/\tau_V = 2.6\%$ , using the Serkowski curve with  $K = 1.15$  and  $\lambda_{\text{max}} = 0.545 \mu\text{m}$ . This is higher than the value of  $P_V/\tau_V = 1.15\%$ , derived by Packham et al. (1997), because of their higher value of  $\tau_t$ . These efficiencies fall in the range of those for the interstellar medium in our Galaxy (Jones 1989).

For Mrk 463E, the spectral index of the degree of polarization ( $\beta = -1.2 \pm 0.2$ ) roughly agrees with that of dichroic absorption, although it is somewhat larger. If we assume that dichroic absorption also dominates for this object,  $\tau_t = 6$ – $9$  and  $P_K/\tau_K = 0.2\%$ – $0.3\%$ , derived in the same way as for NGC 1068 but with  $\beta = 0.33 \pm 0.06$  and  $P_K = 1.7\%$ . These values agree with those derived by Young

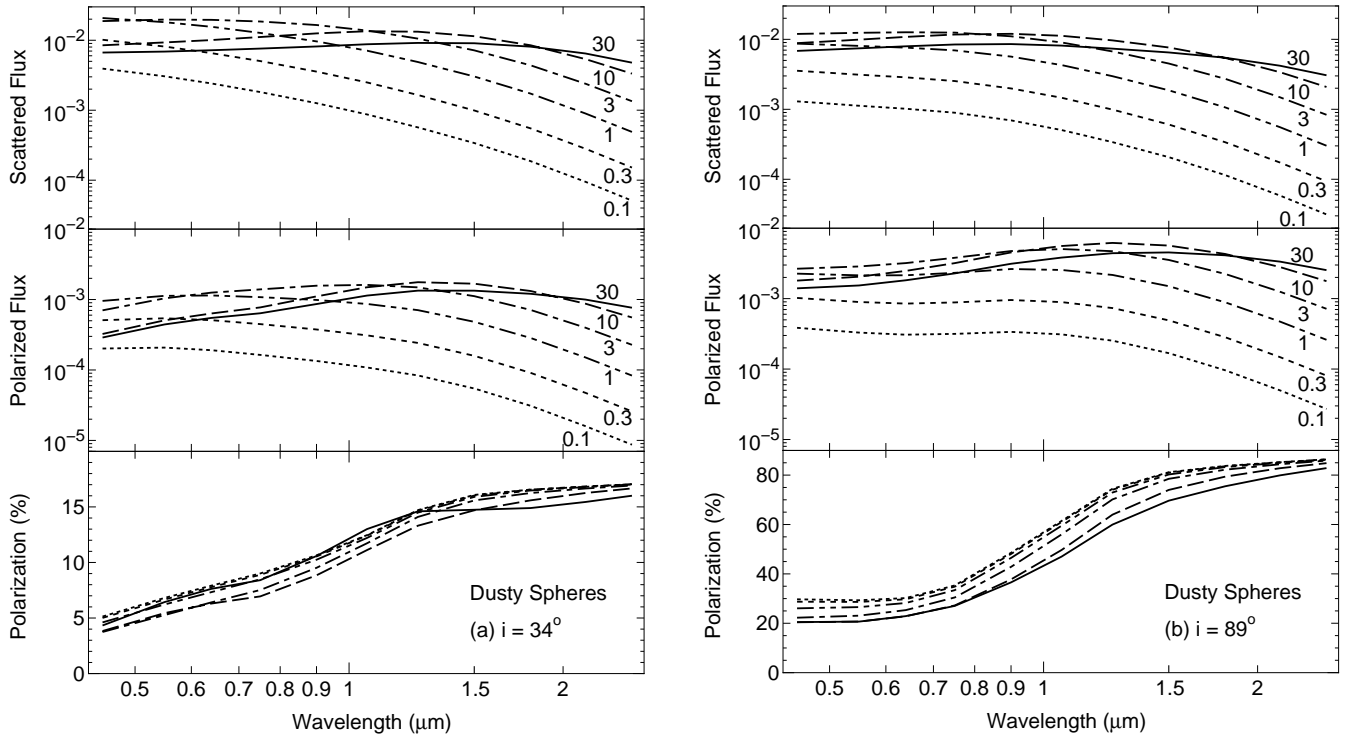


FIG. 9.—Model polarization for scattering in dusty spheres with various optical depths at inclinations of (a)  $34^\circ$  and (b)  $89^\circ$ . The panels are organized as in Fig. 8, but as a function of wavelength. The flux spectra are normalized with the flux spectrum of a nucleus.

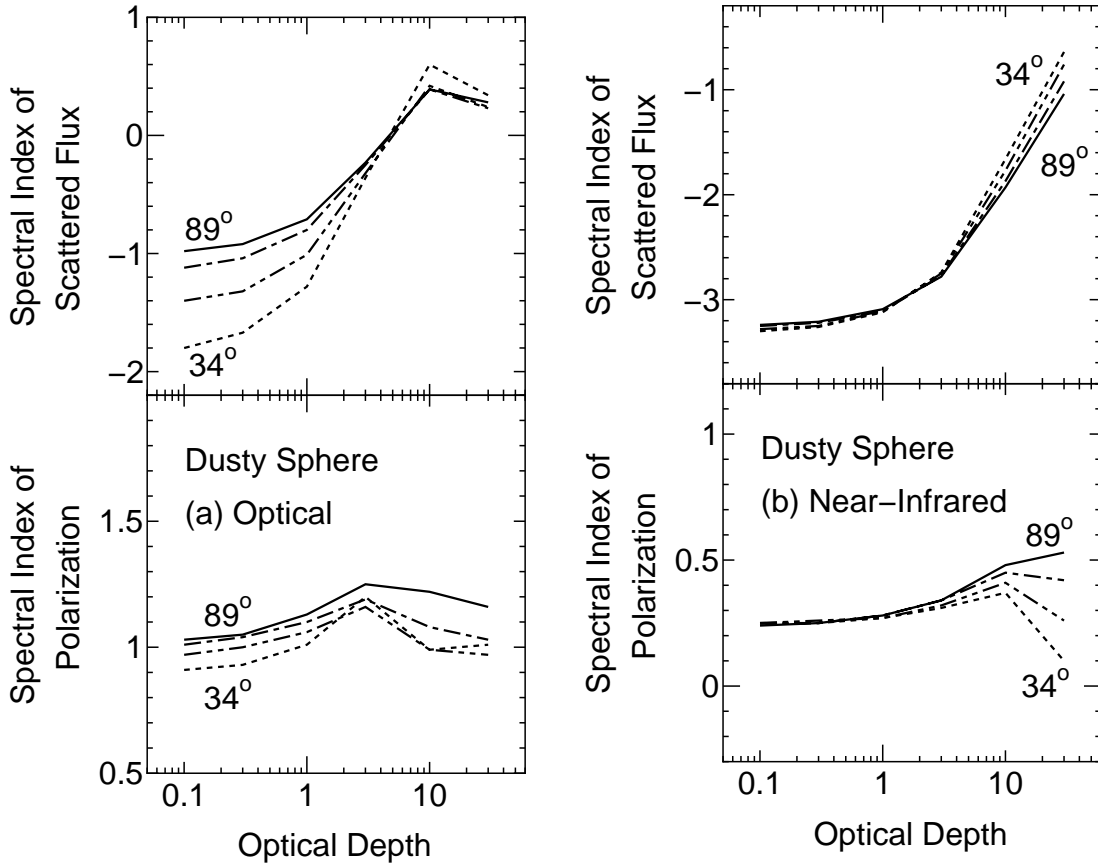


FIG. 10.—Spectral indices of normalized scattered flux (*top*) and degree of polarization spectra (*bottom*) of a dusty sphere as a function of the optical depth (at  $0.55 \mu\text{m}$ ) of the sphere. The indices at the (a) optical and (b) near-infrared regions are shown. These are defined by the fluxes at the two wavelengths,  $0.55$  and  $0.90 \mu\text{m}$  for the optical or  $1.25$  and  $2.15 \mu\text{m}$  for the near-infrared. Each panel shows lines for four inclinations ( $34^\circ$ : short-dashed line;  $51^\circ$ : double-dotted-dashed line;  $68^\circ$ : dot-dashed line; and  $89^\circ$ : solid line).

et al. (1996b), although our value of  $\tau_t$  is smaller than theirs ( $\tau_t = 16$ ).

Unlike NGC 1068 and Mrk 463E, the spectral index of the degree of polarization for Mrk 1210 ( $\beta = 1.3_{-1.8}^{+1.2}$ ) is much higher and distinct from that of dichroic absorption. However, the similar spectral index of the polarized flux to that for NGC 1068 may indicate that the same mechanism does indeed dominate the polarization of both objects, as indicated earlier. A combination of dichroic absorption and electron scattering can produce a higher index for the degree of polarization than dichroic absorption alone. If the scattered light from electrons still dominates the total flux, even in the near-infrared, while the near-infrared polarized flux is mainly from dichroic absorption, the spectral index of the degree of polarization becomes higher. The lower degree of optical polarization in Mrk 1210 than in NGC 1068, is consistent with this assumption. If we assume this combination for Mrk 1210,  $\tau_t \gtrsim 17$ –21 and  $P_K/\tau_K \lesssim 3.7\%$ –4.6% ( $P_K = 8.6\%$ ).

If the optical polarization arises from scattering in the ionization cones and the near-infrared polarization comes from the transmission of radiation through a medium of grains aligned with the local magnetic field, then we are able to infer a relationship between the scattering geometry of the ionization cones and the magnetic field in the torus, as projected onto the sky plane. As the largest change in P.A. between the optical and the near-infrared polarization is  $\sim 20^\circ$  (for NGC 1068), the P.A. of the scattering cones is approximately perpendicular to the direction of the magnetic field.

#### 4.6. Dust Scattering in Torus

Recently, dusty tori with various geometry (such as a cylindrical disk, a tapered disk, and a flared disk) have been modeled to reproduce the infrared emission of AGNs (Pier & Krolik 1992, 1993; Granato & Danese 1994; Stenholm 1994; Efstathiou & Rowan-Robinson 1995; Efstathiou, Hough, & Young 1995; Manske, Henning, & Men'shchikov 1998). Granato et al. (1997) found that moderately thick ( $A_V = 10$ –80) and extended tori are better to explain the infrared spectra of Seyfert nuclei. Fadda et al. (1998) compared these models with the typical spectral energy distribution compiled from a large sample of Seyfert nuclei and found that a flared disk with a size of a few hundred parsecs and a visual extinction of  $A_V = 10$ –30 is most reasonable for both types of Seyfert galaxies.

In this paper we assume a flared disk as the geometry of the torus, as shown in Figure 6c. This is defined by five parameters: the inner radius  $r_{i1}$ , the outer radius  $r_{i2}$ , the half-opening angle  $\theta_t$ , the optical depth along the equatorial plane of the disk  $\tau_t$  measured at  $0.55 \mu\text{m}$ , and the power-law index  $\alpha_t$  for the radial density dependence of dust grains [ $n_t(r) \propto r^{-\alpha_t}$ , where  $n_t(r)$  is the dust number density at the distance  $r$  from the nucleus]. To reduce the free parameters, we fix  $r_{i1} = 1$  pc,  $r_{i2} = 100$  pc,  $\theta_t = 30^\circ$ , and  $\alpha_t = 1$ , which are assumed or found by Manske et al. (1998) in reproducing the spectral energy distribution of NGC 1068. We calculate the polarization for  $\tau_t = 10, 20, 40, 80, 160$ , and 320 at the same wavelengths as in § 4.4.

We note that our treatment of the near-infrared radiative source of Seyfert nuclei is not strictly self-consistent. We assume for simplification that the near-infrared con-

tinuum is radiated from the central point source as well as the optical featureless continuum, but it is actually the thermal radiation from the dusty torus itself. However, the near-infrared emission around  $1$ – $2 \mu\text{m}$  is expected to be radiated from the innermost region with the hottest temperature ( $\sim 1500$  K), and such a region is expected to be much smaller than the whole torus. Laor & Draine (1993) calculated that the radius of such a region with  $T \gtrsim 1000$  K is  $r \sim 1$  pc, when the dust grain is heated by a continuum source with a typical luminosity of a Seyfert galaxy of  $L \sim 10^{37}$  W. Therefore, we expect that this treatment will not produce very different spectra from the strict treatment. If the emitting region is larger, then the degree of polarization would be reduced.

Figures 11a and 11b show the emergent and polarized fluxes and the degree of polarization from the flared disk as a function of inclination. The emergent flux includes the scattered flux and the direct light (unpolarized) through the torus. The optical ( $0.55 \mu\text{m}$ ) emergent and polarized fluxes are very small, as expected for high torus extinctions. These fluxes rapidly decrease at higher inclination, and the degree of polarization increases with inclination. At  $2.15 \mu\text{m}$ , the emergent and polarized fluxes are larger than those at  $0.55 \mu\text{m}$ , as expected from the lower extinctions at this wavelength. Note that the plane of polarization at low  $\tau_t$  and high inclination is different from those in the optical; it is parallel to the polar axis of the torus. It changes to perpendicular at higher  $\tau_t$  or lower inclination. This change of the plane of polarization can be explained as follows. At low  $\tau_t$ , the scattered light from every scatterer in the torus can be observed. The plane of polarization from a disklike distribution of scatterers, especially when viewed edge-on, is parallel to the polar axis (Brown & McLean 1977). As  $\tau_t$  gets higher, the light from the conical surface of the torus begins to dominate in the total light, because the light that has entered the torus is absorbed and cannot reach the outer spherical surface. The plane of polarization from such a cone surface is then perpendicular to the polar axis.

The wavelength dependence of the emergent and polarized flux and the degree of polarization of the torus with various  $\tau_t$  is shown in Figures 12a (inclination of  $34^\circ$ ) and 12b (inclination of  $89^\circ$ ). At  $\tau_t < 160$ , the emergent and polarized fluxes rapidly rise toward the longer wavelength. The degree of polarization rises generally toward the longer wavelength and is higher at higher  $\tau_t$ . Note, however, that the plane of polarization changes from perpendicular to parallel to the polar axis as the wavelength increases. The wavelength at which this change occurs is shorter as  $\tau_t$  gets lower or the inclination gets higher.

The rise of the emergent and polarized fluxes reproduces well the observations of all three nuclei, but they do not show a  $90^\circ$  change in the P.A., having the same position angles in the optical and the near-infrared. The planes of these polarizations are expected to be perpendicular to the polar axis of the nuclei, because the plane of the optical polarization of type 2 Seyfert galaxies is generally perpendicular to the polar axis defined by the radio source structure (Antonucci 1983; Brindle et al. 1990). Indeed, in NGC 1068 and Mrk 463E, the plane of polarization is perpendicular to the polar axis of the nucleus. Therefore, we consider only the perpendicularly polarized components in our model below.

Figures 13a and 13b show the spectral indices of the emergent flux and the degree of the perpendicular polarization

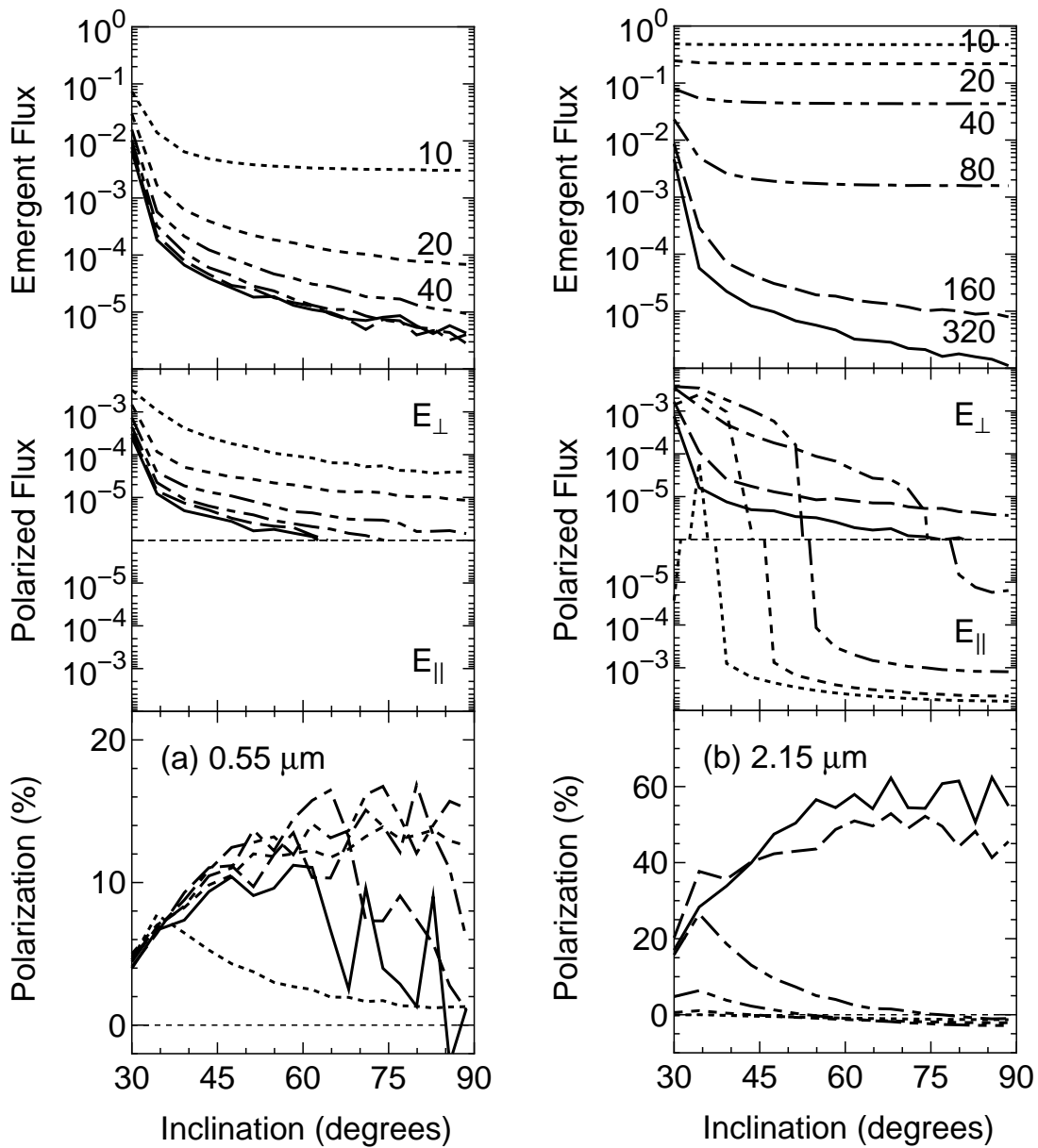


FIG. 11.—Model polarization for scattering in dusty flared disks with various optical depths as a function of inclination at the wavelengths (a)  $\lambda = 0.55$  and (b)  $\lambda = 2.15 \mu\text{m}$ . From top to bottom are the emergent (scattered+direct) and polarized flux and the degree of polarization. The fluxes are normalized with the flux of a nucleus. The middle panel is divided into two sections showing the perpendicular (*top*) and parallel (*bottom*) components to the polar axis of the disk. These components correspond to positive (perpendicular) and negative (parallel) polarization in the bottom panel, respectively. Each panel shows lines for six optical depths of the dusty flared disk at  $0.55 \mu\text{m}$  (10: dotted line; 20: short-dashed line; 40: double-dotted-dashed line; 80: dot-dashed line; 160: long-dashed line; and 320: solid line). The fluctuation in the polarization at higher optical depth is due to errors in the model calculation.

spectra as a function of  $\tau_t$ . In the optical, the index of the emergent flux spectrum decreases sharply as  $\tau_t$  gets higher, reaching 0 at  $\tau_t \sim 160$ . In the near-infrared, it increases with  $\tau_t$  in the low  $\tau_t$  region ( $\tau_t < 40$ ), and then decreases at higher  $\tau_t$  ( $>40$ ); therefore two ranges of  $\tau_t$  exist for moderate spectral indices of the emergent flux ( $\beta \sim 2-5$ ) for each inclination. The spectral index of the degree of polarization increases greatly as  $\tau_t$  gets higher in both the optical and near-infrared. In the optical, it increases across zero, so the degree of polarization rises toward the blue at low  $\tau_t$ , and toward the red at high  $\tau_t$ . In the near-infrared, the index is negative, so the degree of polarization rises toward the shorter wavelength at low  $\tau_t$ . The index approaches zero at high  $\tau_t$ , and then the degree of polarization remains con-

stant with wavelength. The spectral indices of the emergent flux and the degree of polarization are also sensitive to the inclination.

Figures 14a and 14b show the possible spectral indices of the emergent flux and the degree of polarization in our model, together with data for NGC 1068, Mrk 463E, and Mrk 1210. The measured indices of the corrected total flux for these nuclei are normalized, assuming the slope of a typical type 1 Seyfert nucleus to be the incident flux ( $\beta = -1.6$  for the optical, and  $\beta = 0.0$  for the near-infrared). Thus the abscissa readings in Figure 14a are different from the indices in Table 3 by  $-1.6$ .

In the optical, the measured indices of the corrected total fluxes and the degree of polarization of all the three nuclei

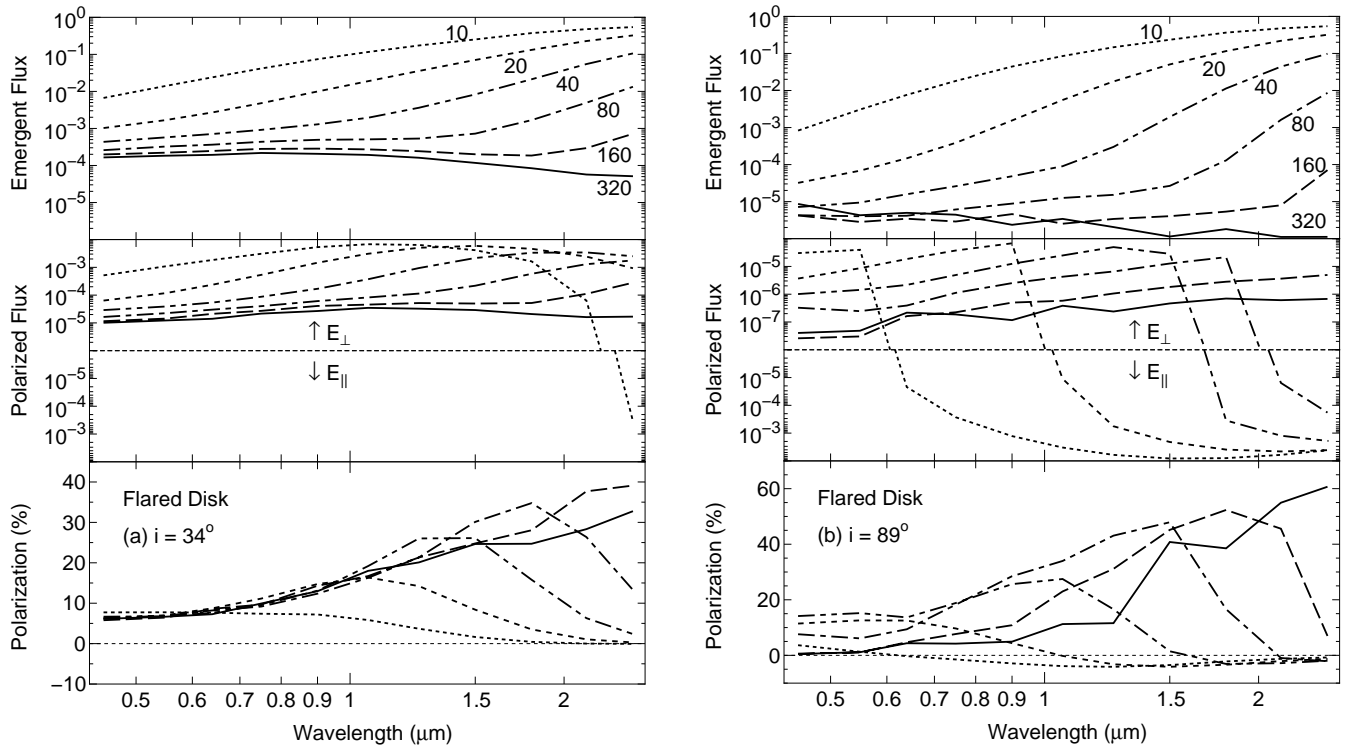


FIG. 12.—Model polarization for scattering in dusty flared disks with various optical depths at the inclinations of (a)  $34^\circ$  and (b)  $89^\circ$ . The panels are organized as in Fig. 11, but as a function of wavelength. The flux spectra are normalized with the flux spectrum of a nucleus.

are distinct from those of the model (Fig. 14a). Therefore, dust scattering in the torus is unlikely to be the dominant mechanism for the optical continuum polarization of these nuclei. Moreover, a contribution from electron scattering is unlikely, because the emergent and polarized fluxes are generally much smaller than that from electron scattering (Fig. 7).

In the near-infrared, the measured indices of the corrected total fluxes and the degree of polarization of all the three nuclei fall in the range of the possible indices in the model (Fig. 14b). For NGC 1068, the torus with  $\tau_t = 40\text{--}100$  and a low inclination of  $34^\circ\text{--}51^\circ$  can produce similar indices to the observations. However, this  $\tau_t$  is rather higher than  $\tau_V \sim 18$  ( $\tau_{0.2\mu\text{m}} \sim 50$ ) derived by Manske et al. (1998) for NGC 1068, while this inclination agrees with the value of  $\sim 40^\circ$  derived from the modeling of the optical and near-infrared polarization of this nucleus (Miller et al. 1991; Young et al. 1995, 1996c; Inglis et al. 1995; Packham et al. 1997). For Mrk 463E, a higher  $\tau_t$  of 120–160 and a higher inclination of  $51^\circ\text{--}68^\circ$  than those for NGC 1068 are required. These higher values arise mainly from the smaller index of the corrected total flux of Mrk 463E than that of NGC 1068. For Mrk 1210,  $\tau_t = 80\text{--}160$  and a low inclination near  $34^\circ$  are required because of the small index of the corrected total flux and the red spectrum of degree of polarization. The combination of  $\tau_t = 160\text{--}320$  and a high inclination near  $90^\circ$  could also produce the similar slope to the observations, and the total and polarized fluxes are much smaller in this case.

The combination with electron scattering in the cones could be considered. However, the contribution from electron scattering is likely to be small in the near-infrared, because the measured indices of the total and polarized flux are very larger than that of a typical type 1 Seyfert nucleus.

## 5. DISCUSSION

As we saw in the previous section, the slopes of the corrected polarization spectra suggest that a combination of electron and dust scattering in ionization cones is most likely to be the dominant mechanism in the *optical* continuum polarization of NGC 1068, Mrk 463E, and Mrk 1210. This agrees well with the previous results (Antonucci & Miller 1985; Miller & Goodrich 1990; Miller et al. 1991; Tran et al. 1992; Tran 1995b; Young et al. 1995; Inglis et al. 1995). On the other hand, dichroic absorption by aligned dust grains in a torus seems to be able to explain the measured spectral slopes of the *near-infrared* continuum polarization of all these nuclei, but dust scattering in a torus can also reproduce these slopes. Here, we discuss if dust scattering in the torus can really explain the near-infrared continuum polarization for these three nuclei.

### 5.1. Very High Optical Thickness?

One important difference between the two models is that the resultant  $\tau_t$  from the slope fitting in the dust-scattering model is much higher than that in the dichroic absorption model. First, let us compare the emergent fluxes of the models with the observations. The measured total fluxes are  $2.8 \times 10^{-13}$ ,  $1.9 \times 10^{-14}$ , and  $2.3 \times 10^{-15} \text{ W m}^{-2} \mu\text{m}^{-1}$  at  $2.15 \mu\text{m}$  for NGC 1068, Mrk 463E, and Mrk 1210, respectively, after correction for starlight dilution. The luminosity of a typical type 1 Seyfert nucleus is  $1.6 \times 10^{36} \text{ W } \mu\text{m}^{-1}$  at  $2.2 \mu\text{m}$  ( $10^{22.4} \text{ W Hz}^{-1}$ ; Fadda et al. 1998). Assuming  $H_0 = 75 \text{ km s}^{-1} \text{ Mpc}^{-1}$  and  $q_0 = 0.5$ , we normalize the measured fluxes with the fluxes of the typical type 1 Seyfert at the same distances. The normalized measured fluxes are 0.49, 5.8, and 0.05 for NGC 1068, Mrk 463E, and Mrk

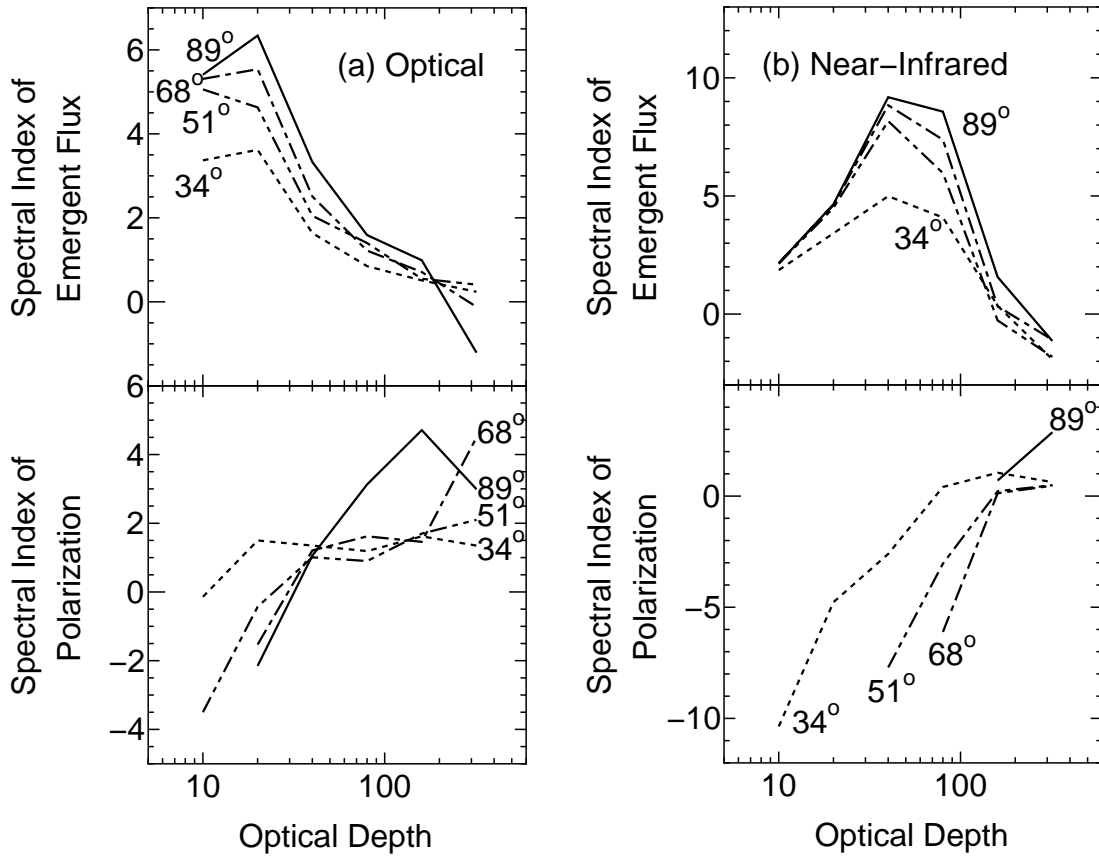


FIG. 13.—Spectral indices of normalized emergent flux (*top*) and degree of polarization spectra (*bottom*) of dusty flared disk as a function of the optical depth (at  $0.55 \mu\text{m}$ ) of the disk. The indices at the (*a*) optical and (*b*) near-infrared regions are shown. These are defined by the fluxes at the two wavelengths,  $0.55$  and  $0.90 \mu\text{m}$  for the optical or  $1.25$  and  $2.15 \mu\text{m}$  for the near-infrared. The indices of only the perpendicular polarized components to the polar axis of the disk are shown in the bottom panels. Each panel shows lines for four inclinations ( $34^\circ$ : *short-dashed line*;  $51^\circ$ : *double-dotted-dashed line*;  $68^\circ$ : *dot-dashed line*; and  $89^\circ$ : *solid line*).

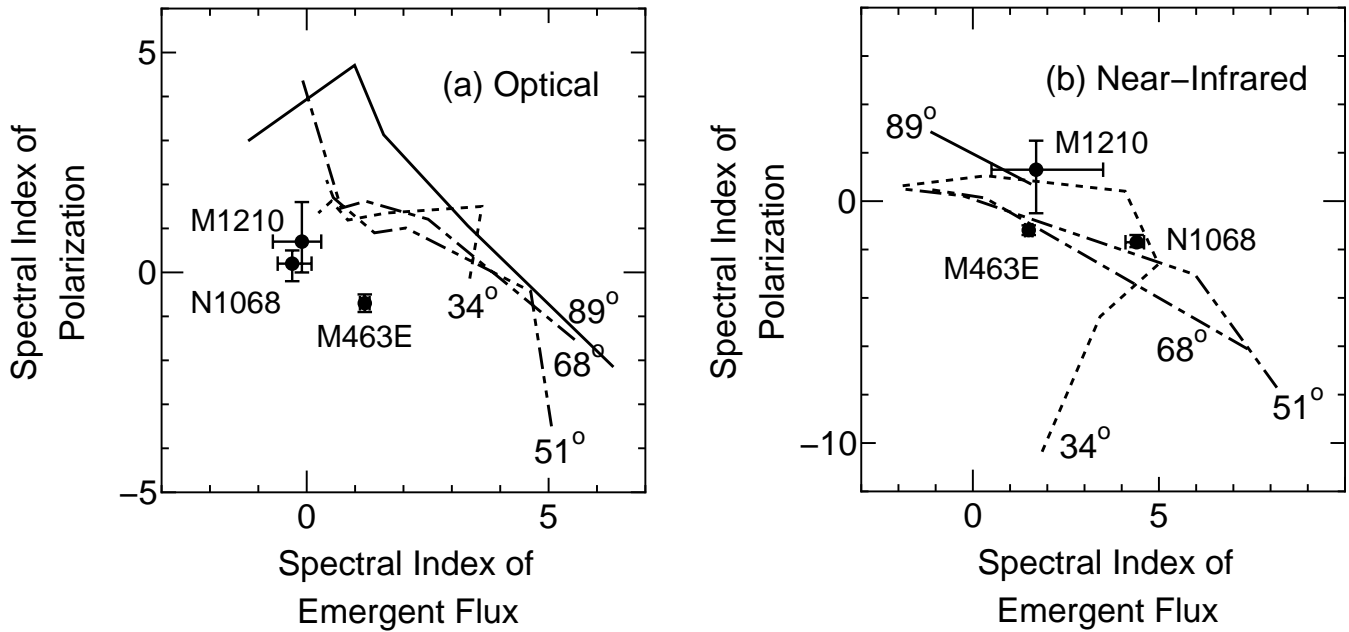


FIG. 14.—Possible spectral indices of normalized emergent flux and degree of polarization for a dusty flared disk. The indices at the (*a*) optical and (*b*) near-infrared regions are shown. Each panel shows lines for four inclination ( $34^\circ$ : *short-dashed line*;  $51^\circ$ : *double-dotted-dashed line*;  $68^\circ$ : *dot-dashed line*; and  $89^\circ$ : *solid line*). The upper left-hand end point of each line represents the indices at  $\tau_t = 320$ , and another end point represents those at the lowest  $\tau_t$  shown in Fig. 13 (*bottom panels*). The filled circles with error bars are the observed spectral indices of the three nuclei. The observed indices are normalized with the slope of the spectrum of a typical type 1 Seyfert nucleus.

1210, respectively. However, according to Mazzarella et al. (1991), Mrk 463E has a near-infrared luminosity comparable to Palomar-Green (PG) quasars rather than to a type 1 Seyfert nucleus. The median luminosity of PG quasars is  $2.3 \times 10^{37} \text{ W } \mu\text{m}^{-1}$  at  $2.2 \mu\text{m}$  ( $\nu L_\nu = 1.3 \times 10^{11} L_\odot$ ; Mazzarella et al. 1991). If we adopt this luminosity for Mrk 463E, the normalized measured flux is then 0.40. Our estimated optical depths of the tori in the dust-scattering model lead to much smaller fluxes than the measured ones; fluxes of the order of 0.01, 0.0001, and 0.001 are derived for NGC 1068, Mrk 463E, and Mrk 1210, respectively. In contrast, the smaller optical depths in the dichroic absorption model lead to the emergent fluxes consistent with the measured fluxes; the normalized emergent fluxes of  $0.13 \pm 0.02$ ,  $0.34\text{--}0.49$ , and  $\leq 0.08\text{--}0.13$  are derived for NGC 1068, Mrk 463E, and Mrk 1210, respectively.

Second, we will compare the degree of polarization itself, not its spectral index, of the dust-scattering model with the observations. The degree of polarization from the model torus ( $P = 5\%\text{--}30\%$  at  $2.15 \mu\text{m}$ ) is substantially higher than the observation of NGC 1068 ( $P = 4.7\%$ ). Similarly, high  $\tau_t$  and inclination produce much higher degrees of polarization ( $P = 25\%\text{--}50\%$ ) than the observed starlight-corrected degrees of polarization of Mrk 463E and Mrk 1210 ( $P = 1.7\%$  and  $8.6\%$ ).

Thus the dust scattering in tori with optical thickness  $\tau_t$  higher than 40 (NGC 1068), 120 (Mrk 463E), and 80 or 160 (Mrk 1210) cannot explain the near-infrared flux for these nuclei. Such high optical depths of  $\tau_t > 40$  have been required because the observations imply small negative spectral indices for the degree of polarization ( $\beta$  is  $-1.7$ ,  $-1.2$ , and  $1.3$  for these nuclei) while such spectral indices are only realized when the optical depth is sufficiently high (see Fig. 13*b*), in the current model.

### 5.2. Possible Dust-Scattering Model

To reproduce the measured total fluxes at  $2.2 \mu\text{m}$  and spectral indices ( $\beta \sim 2\text{--}5$ ) between  $1.2$  and  $2.2 \mu\text{m}$  by our scattering model, moderate optical depths of  $\tau_t = 10\text{--}40$  are required for all the three nuclei (see Fig. 11*b* and Fig. 13*b*, *top panel*). The tori with such moderate  $\tau_t$ , however, produce steeper slopes of the degree of polarization spectrum than the observations (see Fig. 13*b*, *bottom panel*). This rapid decrease in the model is mainly due to the rapid rise of the direct light through the torus relative to the slow rise, or even decrease when  $\tau_t$  is very low ( $\sim 10$ ), of the scattered light toward the longer wavelength. These variations of the scattered and direct light in the emergent fluxes from our flared disks are clearly shown in Figure 15. This slow rise of the scattered flux is due to the decrease of the albedo of dust grains (Draine & Lee 1984) longward of  $1 \mu\text{m}$ . The decrease of the scattering cross section as the extinction drops also reduces the scattered flux at the longer wavelength at the low extinction ( $\tau_\lambda < 2$ ; Code & Whitney 1995). This variation of the flux with wavelength depends mainly on the scattering properties of the dust and depends less on the geometry of the flared disk.

The failure of our scattering models in fitting both the near-infrared total flux and the spectral slope of degree of polarization demonstrates that a torus whose dust has a similar composition and similar size distribution to that in the Galactic diffuse interstellar medium cannot explain the near-infrared radiation for NGC 1068, Mrk 463E, and Mrk 1210.

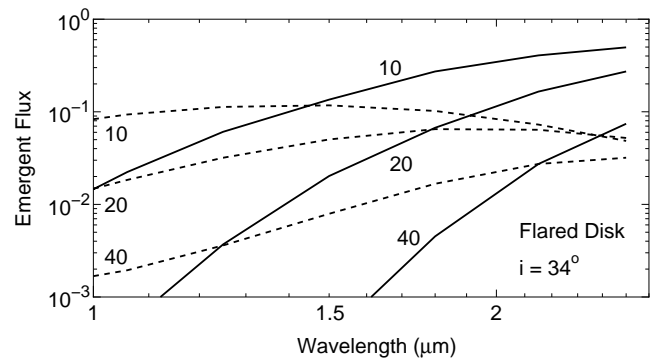


FIG. 15.—Scattered (*dashed lines*) and direct light (*solid lines*) from dusty flared disks as a function of wavelength at the inclination of  $34^\circ$ . The optical depths (at  $0.55 \mu\text{m}$ ) of the disks are labeled by the numbers. The flux spectra are normalized with the flux spectrum of a nucleus.

In fact, recent observational results suggest that the grain size distribution in the circumnuclear region of AGNs is biased toward large values (Laor & Draine 1993; Maiolino et al. 2001*b*; Maiolino, Marconi, & Oliva 2001*a*). Such a size distribution can make the spectral slope of the degree of polarization between  $1.2$  and  $2.2 \mu\text{m}$  flatter, because it makes the extinction curve flatter (Laor & Draine 1993) and keeps a significant albedo longward of  $1 \mu\text{m}$  (Weingartner & Draine 2001). The dominance of large grains would also change the peak polarization in Figure 5 (*top panel*). In the current model, the slope of the peak polarization between  $1.2$  and  $2.2 \mu\text{m}$  is rather flat. If the size of grains increases, the steep slope around  $1 \mu\text{m}$  will move toward the longer wavelength. When it comes in the  $1.2\text{--}2.2 \mu\text{m}$  range, for which the near-infrared spectral index is calculated, the index of the degree of polarization will be larger, so that moderate  $\tau_t$  models might be able to reproduce the observed slow decrease of polarization with wavelengths.

The moderate  $\tau_t$  are consistent with  $\tau_t = 9\text{--}28$  ( $A_V = 10\text{--}30$ ), as derived by Fadda et al. (1998) from a comparison of their torus models with a typical spectral energy distribution of Seyfert nuclei. These moderate  $\tau_t$  are also consistent with  $\tau_t \sim 18$  ( $\tau_{0.2\mu\text{m}} \sim 50$ ) derived by Manske et al. (1998), when using similar torus parameters to our ones, for NGC 1068. The detection of the near-infrared broad emission lines ( $\text{Pa}\beta$ ,  $\text{Br}\gamma$ ) in the total flux spectra of Mrk 463E and Mrk 1210 (Goodrich et al. 1994; Ruiz et al. 1994; Veilleux, Goodrich, & Hill 1997) also supports moderate optical depths for the torus,  $\tau_t = 10\text{--}40$ , rather than  $\tau_t \gtrsim 40$ . Goodrich et al. (1994) and Veilleux et al. (1997) estimated the extinction toward BLRs,  $\tau_V \gtrsim 5\text{--}9$  (for  $\text{Pa}\beta$ ) and  $\tau_V \gtrsim 4\text{--}6$  (for  $\text{Br}\gamma$ ) for these nuclei from the ratios of the broad components in these lines and  $\text{H}\alpha$ , assuming case B recombination and the standard Galactic extinction curve. Thus, although we should be careful about using these estimates of the extinction because a substantial fraction of the line emission could be scattered light and the determination of the fraction is difficult, these extinction values derived from the near-IR emission lines are fairly low. On the other hand, the nondetection of such broad-line components in NGC 1068 (Thompson, Lebofsky, & Rieke 1978; Hall et al. 1981; DePoy 1987; Veilleux et al. 1997; Lutz et al. 2000) suggests rather high extinction (e.g.,  $\tau_V > 50$ ; Lutz et al. 2000) toward BLRs for this nucleus. However, the strengths of dust absorption features again support the moderate  $\tau_t$ ,

even for NGC 1068. Roche et al. (1984) and Tomono et al. (2001) measured the strength of the  $9.7 \mu\text{m}$  silicate absorption feature in this nucleus and derived dust extinctions of  $\tau_V \sim 7$  and  $\tau_V = 7\text{--}21$ , respectively. Bridger, Wright, & Geballe (1994) and Imanishi et al. (1997) also observed the C-H band absorption at  $3.4 \mu\text{m}$  in this nucleus and derived dust extinctions of  $\tau_V \sim 20$  and  $\tau_V = 17\text{--}28$ , respectively. This disagreement of the extinction derived from the absorption features with those from the broad-line detection may indicate that BLRs are more obscured than the infrared-emitting regions in NGC 1068. Our  $\tau_i$  represents the extinction toward the near-infrared-emitting regions rather than toward BLRs, so it should agree with the extinction derived from the absorption features.

Dust scattering in a torus dominated by large grains could also explain the mid-infrared polarization of type 2 Seyfert nuclei. Bailey et al. (1988) presented the broadband polarimetry of NGC 1068 over the wavelength range of  $0.36\text{--}4.8 \mu\text{m}$ . They showed that the P.A. of polarization changes greatly ( $\sim 70^\circ$ ) between  $4$  and  $5 \mu\text{m}$  and the degree of polarization at  $4.8 \mu\text{m}$  is  $\sim 0.9\%$ . Aitken et al. (1984) also showed that this nucleus has a polarization with  $1\%\text{--}2\%$  between  $8$  and  $13 \mu\text{m}$  and the P.A. is similar to that at  $4.8 \mu\text{m}$ . Bailey et al. (1988) suggest that this polarization over the wavelength range of  $4\text{--}13 \mu\text{m}$  is due to thermal emission from aligned grains. According to Efstathiou et al. (1996) and Efstathiou, McCall, & Hough (1997), the change in P.A. suggests that the dominant polarization mechanism changes from dichroic absorption to emission by aligned grains between  $4$  and  $5 \mu\text{m}$ . However, dust scattering in the torus can also reproduce a similar change in P.A. around these wavelengths. Although the grain size distribution for the diffuse interstellar medium leads to very small scattered and polarized fluxes at these wavelengths, because of the small albedo (Draine & Lee 1984), a dust composition dominated by large grains could produce significant scattered and polarized fluxes even at these wavelengths.

Thus, dust scattering in the torus of moderate optical depth dominated by large grains might provide a reasonable explanation for the near-infrared radiation from Seyfert nuclei, but pursuing it is beyond the scope of the current investigation.

Lumsden et al. (1999) presented a near-infrared high-resolution polarization map of the nucleus of NGC 1068. They showed that the *K*-band polarization map has no centrosymmetric scattering pattern, unlike the maps at shorter wavelengths such as the *J* band and the optical. Therefore, they suggested dichroic absorption by aligned dust grains as polarization mechanism for the near-infrared polarization, because the single-scattered light of a single point source cannot reproduce such a noncentrosymmetric scattering pattern. However, Simpson et al. (2002) noted that the polarized light could include the multiply scattered light in both cones and torus (or disk), such as light backscattered from the cones and scattered a second time in the torus. They presented a more highly resolved polarization image of NGC 1068 at  $2 \mu\text{m}$ , taken by NICMOS Camera 2 on the *Hubble Space Telescope* (*HST*). They showed that there would be a small contribution from off-nuclear scattered light to the polarized flux within a  $2''$  aperture. In this paper, for simplification, we have calculated the polarization from the cones and the torus separately. However, to model the polarization pattern, we would need to model the combination of these components. Also, an extended radiative

source could be needed, because recent near-infrared high-resolution imaging of the nucleus of NGC 1068 show an emission region extending a few tens of parsecs at  $2 \mu\text{m}$  (e.g., Weinberger, Neugebauer, & Matthews 1999).

## 6. CONCLUSIONS

We have presented optical to near-infrared spectropolarimetry of four type 2 Seyfert nuclei. The slope of the degree of optical continuum polarization after correction for starlight dilution is almost zero for NGC 1068, Mrk 463E, and Mrk 1210. This result is consistent with the previous suggestion that electron scattering is the principal polarization mechanism for the optical continuum polarization for these nuclei. The deviation of the slope from zero suggests significant contributions of dust scattering in the optical continuum polarization of the nuclei of Mrk 463E and Mrk 1210.

For the near-infrared, we found that dichroic absorption by aligned dust grains can explain the continuum polarization of the nuclei of Mrk 1210 and Mrk 463E as well as NGC 1068. Assuming a typical spectral slope of type 1 Seyfert nuclei ( $\beta \sim 0$ ) as a background source, we have estimated the visual optical depth of the torus on the order of  $10\text{--}20$  for these nuclei from the spectral slope of the polarized flux.

We have also presented a polarization model for dust scattering in a torus with the same grain size distribution as in the Galactic diffuse interstellar medium and a flared disk geometry, making an attempt to reproduce the near-infrared continuum polarization of these nuclei. We found that this model cannot reproduce the observed spectral slope of the near-infrared polarization and total flux of these nuclei simultaneously. This model requires very high visual optical depths for the torus of the order of  $40\text{--}160$  to reproduce the spectral slope of polarization, while it requires a moderate visual optical depth of the order of  $10\text{--}40$  to reproduce the total flux. However, this might only indicate that the grain size distribution in the torus of AGNs is different from in our Galaxy. Dust scattering in a torus with moderate optical depth and dominated by large grains might provide a reasonable explanation for the near-infrared radiation from AGNs.

We thank the staff of the UKIRT for their support in the observations. We also thank the staff of the Subaru Telescope for help in preparing the instrument and the discussion. We are grateful to the members of our laboratory for the discussion and encouragement. We also thank J. Smith for kindly providing his analytical scattering code and the anonymous referee for helpful suggestions. The United Kingdom Infrared Telescope is operated by the Joint Astronomy Centre on behalf of the UK Particle Physics and Astronomy Research Council. We thank the Department of Physical Sciences, University of Hertfordshire for providing IRPOL2 for the UKIRT. This research has made use of the NASA/IPAC Extragalactic Database (NED), which is operated by the Jet Propulsion Laboratory, California Institute of Technology, under contract with the National Aeronautics and Space Administration. This work was financially supported in part by a Grant-in-Aid for Scientific Research of the Ministry of Education, Culture, Sports, Science, and Technology.

## REFERENCES

- Aitken, D. K., Bailey, J. A., Briggs, G., Hough, J. H., & Roche, P. F. 1984, *Nature*, 310, 660
- Alexander, D. M., Young, S., & Hough, J. H. 1999, *MNRAS*, 304, L1
- Alonso-Herrero, A., Quillen, A. C., Simpson, C., Efstathiou, A., & Ward, M. J. 2001, *AJ*, 121, 1369
- Angel, J. R. P., Stockman, H. S., Woolf, N. J., Beaver, E. A., & Martin, P. G. 1976, *ApJ*, 206, L5
- Antonucci, R. R. J. 1983, *Nature*, 303, 158
- . 1993, *ARA&A*, 31, 473
- Antonucci, R. R. J., & Miller, J. S. 1985, *ApJ*, 297, 621
- Bailey, J., Axon, D. J., Hough, J. H., Ward, M. J., McLean, I., & Heathcote, S. R. 1988, *MNRAS*, 234, 899
- Bhoren, C. F., & Huffman, D. R. 1983, *Absorption and Scattering of Light by Small Particles* (New York: Wiley)
- Bianchi, S., Ferrara, A., & Giovanardi, C. 1996, *ApJ*, 465, 127
- Blanco, P. R., Ward, M. J., & Wright, G. S. 1990, *MNRAS*, 242, 4P
- Bridger, A., Wright, G. S., & Geballe, T. R. 1994, in *Infrared Astronomy with Arrays*, ed. I. S. McLean (Dordrecht: Kluwer), 537
- Brindle, C., Hough, J. H., Bailey, J. A., Axon, D. J., Ward, M. J., Sparks, W. B., & McLean, I. S. 1990, *MNRAS*, 244, 577
- Brown, J. C., & McLean, I. S. 1977, *A&A*, 57, 141
- Cardelli, J. A., Clayton, G. C., & Mathis, J. S. 1989, *ApJ*, 345, 245
- Code, A. D., & Whitney, B. A. 1995, *ApJ*, 441, 400
- DePoy, D. L. 1987, in *Infrared Astronomy with Arrays*, ed. C. G. Wynn-Williams, E. E. Becklin, & L. H. Good (Honolulu: Univ. Hawaii, Inst. Astron.), 426
- Draine, B. T. 1985, *ApJS*, 57, 587
- Draine, B. T., & Lee, H. M. 1984, *ApJ*, 285, 89
- Efstathiou, A., Hough, J. H., McCall, A., & Young, S. 1996, in *ASP Conf. Ser. 97, Polarimetry of the Interstellar Medium*, ed. W. G. Roberge & D. C. B. Whittet (San Francisco: ASP), 602
- Efstathiou, A., Hough, J. H., & Young, S. 1995, *MNRAS*, 277, 1134
- Efstathiou, A., McCall, A., & Hough, J. H. 1997, *MNRAS*, 285, 102
- Efstathiou, A., & Rowan-Robinson, M. 1995, *MNRAS*, 273, 649
- Fadda, D., Giuricin, G., Granato, G. L., & Vecchies, D. 1998, *ApJ*, 496, 117
- Fischer, O., Henning, Th., & Yorke, H. W. 1994, *A&A*, 284, 187
- Francis, P. J., Hewett, P. C., Foltz, C. B., Chaffee, F. H., Weymann, R. J., & Morris, S. L. 1991, *ApJ*, 373, 465
- Goodrich, R. W. 1992, *ApJ*, 399, 50
- Goodrich, R. W., Veilleux, S., & Hill, G. J. 1994, *ApJ*, 422, 521
- Granato, G., & Danese, L. 1994, *MNRAS*, 268, 235
- Granato, G. L., Danese, L., & Franceschini, A. 1997, *ApJ*, 486, 147
- Hall, D. N. B., Kleinmann, S. G., Scoville, N. Z., & Ridgway, S. T. 1981, *ApJ*, 248, 898
- Heiles, C. 2000, *AJ*, 119, 923
- Hines, D. C., Schmidt, G. D., Gordon, K. D., Smith, P. S., Wills, B. J., Allen, R. G., & Sitko, M. L. 2001, *ApJ*, 563, 512
- Hutchings, J. B., & Neff, S. G. 1989, *AJ*, 97, 1306
- Imanishi, M., Terada, H., Sugiyama, K., Motohara, K., Goto, M., & Maihara, T. 1997, *PASJ*, 49, 69
- Inglis, M. D., Young, S., Hough, J. H., Gledhill, T., Axon, D. J., Bailey, J. A., & Ward, M. J. 1995, *MNRAS*, 275, 398
- Jones, T. J. 1989, *ApJ*, 346, 728
- Kartje, J. F. 1995, *ApJ*, 452, 565
- Kay, L. E. 1994, *ApJ*, 430, 196
- Laor, A., & Draine, B. T. 1993, *ApJ*, 402, 441
- Lumsden, S. L., Moore, T. J. T., Smith, C., Fujiyoshi, T., Bland-Hawthorn, J., & Ward, M. J. 1999, *MNRAS*, 303, 209
- Lutz, D., et al. 2000, *ApJ*, 530, 733
- Maiolino, R., Marconi, A., & Oliva, E. 2001, *A&A*, 365, 37
- Maiolino, R., Marconi, A., Salvati, M., Risaliti, G., Severgnini, P., Oliva, E., La Franca, F., & Vanzì, L. 2001, *A&A*, 365, 28
- Mannucci, F., Basile, F., Poggianti, B. M., Cimatti, A., Daddi, E., Pozzetti, L., & Vanzì, L. 2001, *MNRAS*, 326, 745
- Manske, V., Henning, Th., & Men'shchikov, A. B. 1998, *A&A*, 331, 52
- Manzini, A., & di Serego Alighieri, S. 1996, *A&A*, 311, 79
- Martin, P. G., & Whittet, D. C. B. 1990, *ApJ*, 357, 113
- Martin, P. G., et al. 1992, *ApJ*, 392, 691
- Mathis, J. S., Rumpl, W., & Nordsieck, K. H. 1977, *ApJ*, 217, 425
- Mazzarella, J. M., Gaume, R. A., Soifer, B. T., Graham, J. R., Neugebauer, G., & Matthews, K. 1991, *AJ*, 102, 1241
- McAlary, C. W., & Rieke, G. H. 1988, *ApJ*, 333, 1
- McLean, I. S., Aspin, C., Heathcote, S. R., & McCaughrean, M. J. 1983, *Nature*, 304, 609
- Miller, J. S., & Antonucci, R. J. 1983, *ApJ*, 271, L7
- Miller, J. S., & Goodrich, R. W. 1990, *ApJ*, 355, 456
- Miller, J. S., Goodrich, R. W., & Mathews, W. G. 1991, *ApJ*, 378, 47
- Nagata, T. 1990, *ApJ*, 348, L13
- Nagata, T., Kobayashi, N., & Sato, S. 1994, *ApJ*, 423, L113
- Packham, C., Young, S., Hough, J. H., Axon, D. J., & Bailey, J. A. 1997, *MNRAS*, 288, 375
- Pickles, A. J. 1998, *PASP*, 110, 863
- Pier, E. A., & Krolik, J. H. 1992, *ApJ*, 401, 99
- . 1993, *ApJ*, 418, 673
- Rix, H.-W., Carleton, N. P., Rieke, G., & Rieke, M. 1990, *ApJ*, 363, 480
- Roche, P. F., Aitken, D. K., Phillips, M. M., & Whitmore, B. 1984, *MNRAS*, 207, 35
- Ruiz, M., Rieke, G. H., & Schmidt, G. D. 1994, *ApJ*, 423, 608
- Sato, S. 2000, *UKIRT Newsl.*, 7, 12
- Schlegel, D. J., Finkbeiner, D. P., & Davis, M. 1998, *ApJ*, 500, 525
- Serkowski, K., Mathewson, D. S., & Ford, V. L. 1975, *ApJ*, 196, 261
- Simpson, J. P., Colgan, S. W. J., Erickson, E. F., Hines, D. C., Schultz, A. S. B., & Trammell, S. R. 2002, *ApJ*, 574, 95
- Stenholm, L. 1994, *A&A*, 290, 393
- Thompson, R. I., Lebofsky, M. J., & Rieke, G. H. 1978, *ApJ*, 222, L49
- Tomono, D., Doi, Y., Usuda, T., & Nishimura, T. 2001, *ApJ*, 557, 637
- Tran, H. D. 1995a, *ApJ*, 440, 565
- . 1995b, *ApJ*, 440, 578
- Tran, H. D., Miller, J. S., & Kay, L. E. 1992, *ApJ*, 397, 452
- Tremonti, C. A., Uomoto, A., Antonucci, R. R. J., Tsvetanov, Z. I., Ford, H. C., & Kriss, G. A. 1996, *BAAS*, 28, 1287
- Uomoto, A., Caganoff, S., Ford, H. C., Rosenblatt, E. I., Antonucci, R. R. J., Evans, I. N., & Chohen, R. D. 1993, *AJ*, 105, 1308
- Vanden Berk, D. E., et al. 2001, *AJ*, 122, 549
- Veilleux, S., Goodrich, R. W., & Hill, G. J. 1997, *ApJ*, 477, 631
- Weinberger, A. J., Neugebauer, G., & Matthews, K. 1999, *AJ*, 117, 2748
- Weingartner, J. C., & Draine, B. T. 2001, *ApJ*, 548, 296
- White, R. L. 1979, *ApJ*, 229, 954
- Whittet, D. C. B., Martin, P. G., Hough, J. H., Rouse, M. F., Bailey, J. A., & Axon, D. J. 1992, *ApJ*, 386, 562
- Whittet, D. C. B., & van Breda, I. G. 1978, *A&A*, 66, 57
- Wilking, B. A., Lebofsky, M. J., Martin, P. G., Rieke, G. H., & Kemp, J. C. 1980, *ApJ*, 235, 905
- Witt, A. N. 1977, *ApJS*, 35, 1
- Wilson, A. S. 1996, *Vistas Astron.*, 40, 63
- Wolf, S., & Henning, Th. 1999, *A&A*, 341, 675
- Young, S., Hough, J. H., Axon, D. J., Bailey, J. A., & Ward, M. J. 1995, *MNRAS*, 272, 513
- Young, S., Hough, J. H., Axon, D. J., Ward, M. J., & Bailey, J. A. 1996a, *MNRAS*, 280, 291
- Young, S., Hough, J. H., Efstathiou, A., Wills, B. J., Bailey, J. A., & Axon, D. J. 1996b, *MNRAS*, 281, 1206
- Young, S., Packham, C., Hough, J. H., & Efstathiou, A. 1996c, *MNRAS*, 283, L1